

# *Skill assessment and sources of predictability for the leading modes of sub-seasonal Eastern Africa short rains variability*

Article

Accepted Version

de Andrade, F. M., Hiron, L. C. ORCID: <https://orcid.org/0000-0002-1189-7576> and Woolnough, S. J. ORCID: <https://orcid.org/0000-0003-0500-8514> (2024) Skill assessment and sources of predictability for the leading modes of sub-seasonal Eastern Africa short rains variability. *Climate Dynamics*, 62. pp. 5721-5737. ISSN 1432-0894 doi: 10.1007/s00382-024-07244-9 Available at <https://centaur.reading.ac.uk/116132/>

It is advisable to refer to the publisher's version if you intend to cite from the work. See [Guidance on citing](#).

To link to this article DOI: <http://dx.doi.org/10.1007/s00382-024-07244-9>

Publisher: Springer

the [End User Agreement](#).

[www.reading.ac.uk/centaur](http://www.reading.ac.uk/centaur)

**CentAUR**

Central Archive at the University of Reading

Reading's research outputs online

# Metadata of the article that will be visualized in OnlineFirst

ArticleTitle	Skill assessment and sources of predictability for the leading modes of sub-seasonal Eastern Africa short rains variability	
Article Sub-Title		
Article CopyRight	The Author(s), under exclusive licence to Springer-Verlag GmbH Germany, part of Springer Nature (This will be the copyright line in the final PDF)	
Journal Name	Climate Dynamics	
Corresponding Author	FamilyName Particle Given Name Suffix Division Organization Address Division Organization Address Phone Fax Email URL ORCID	<b>Andrade</b> de <b>Felipe M.</b> National Centre for Atmospheric Science and Department of Meteorology University of Reading Reading, UK National Institute for Space Research Cachoeira Paulista, SP, Brazil felipestratus@gmail.com <a href="http://orcid.org/0000-0001-6653-3916">http://orcid.org/0000-0001-6653-3916</a>
Author	FamilyName Particle Given Name Suffix Division Organization Address Phone Fax Email URL ORCID	<b>Hirons</b> <b>Linda C.</b> National Centre for Atmospheric Science and Department of Meteorology University of Reading Reading, UK <a href="http://orcid.org/0000-0002-1189-7576">http://orcid.org/0000-0002-1189-7576</a>
Author	FamilyName Particle Given Name Suffix Division Organization Address Phone Fax Email URL ORCID	<b>Woolnough</b> <b>Steven J.</b> National Centre for Atmospheric Science and Department of Meteorology University of Reading Reading, UK <a href="http://orcid.org/0000-0003-0500-8514">http://orcid.org/0000-0003-0500-8514</a>
Schedule	Received Revised	8 Jan 2024

## Abstract

Understanding how models represent sub-seasonal rainfall variations and what influences model skill is essential for improving sub-seasonal forecasts and their applications. Here, empirical orthogonal function (EOF) analysis is employed to investigate weekly Eastern Africa short rains variability from October to December. The observed leading EOF modes are identified as (i) a monopole-like rainfall pattern with anomalies impacting southern Ethiopia, Kenya, and northern Tanzania; and (ii) a dipole-like rainfall pattern with contrasting anomalies between Tanzania and the northeastern sector of Eastern Africa. An examination of the links between the leading modes and specific climate drivers, namely, the Madden–Julian Oscillation (MJO), El Niño–Southern Oscillation, and Indian Ocean Dipole (IOD), shows that the MJO and IOD have the highest correlations with the two rainfall modes and indicates that the monopole (dipole)-like rainfall pattern is associated with MJO convective anomalies in the tropical Indian Ocean and western Pacific (Maritime Continent and Western Hemisphere). Assessments of model ability to capture and predict the leading modes show that the European Centre for Medium-Range Weather Forecasts (ECMWF) and the UK Met Office models outperform the National Centers for Environmental Prediction model at forecast horizons from one to four weeks ahead. Amongst the drivers examined, the MJO has the largest impact on the forecast skill of rainfall modes within the ECMWF model. If MJO-related variability is reliably represented, the ECMWF model is more skilful at predicting the main modes of weekly rainfall variability over the region. Our findings can support model developments and enhance anticipatory planning efforts in several sectors, such as agriculture, food security, and energy.

---

Keywords (separated by '-') Eastern Africa Short Rains - Empirical Orthogonal Function Analysis - Madden–Julian Oscillation - El Niño–Southern Oscillation - Indian Ocean Dipole - Sub-seasonal Prediction Skill

---

Footnote Information

---



# 1 Skill assessment and sources of predictability for the leading modes 2 of sub-seasonal Eastern Africa short rains variability

3 Felipe M. de Andrade<sup>1,2</sup> · Linda C. Hirons<sup>1</sup> · Steven J. Woolnough<sup>1</sup>

4 Received: 8 January 2024 / Accepted: 12 April 2024

5 © The Author(s), under exclusive licence to Springer-Verlag GmbH Germany, part of Springer Nature 2024

## 6 Abstract

7 Understanding how models represent sub-seasonal rainfall variations and what influences model skill is essential for improving  
8 sub-seasonal forecasts and their applications. Here, empirical orthogonal function (EOF) analysis is employed to investigate  
9 weekly Eastern Africa short rains variability from October to December. The observed leading EOF modes are identified  
10 as (i) a monopole-like rainfall pattern with anomalies impacting southern Ethiopia, Kenya, and northern Tanzania; and (ii)  
11 a dipole-like rainfall pattern with contrasting anomalies between Tanzania and the northeastern sector of Eastern Africa.  
12 An examination of the links between the leading modes and specific climate drivers, namely, the Madden–Julian Oscilla-  
13 tion (MJO), El Niño–Southern Oscillation, and Indian Ocean Dipole (IOD), shows that the MJO and IOD have the highest  
14 correlations with the two rainfall modes and indicates that the monopole (dipole)-like rainfall pattern is associated with  
15 MJO convective anomalies in the tropical Indian Ocean and western Pacific (Maritime Continent and Western Hemisphere).  
16 Assessments of model ability to capture and predict the leading modes show that the European Centre for Medium-Range  
17 Weather Forecasts (ECMWF) and the UK Met Office models outperform the National Centers for Environmental Prediction  
18 model at forecast horizons from one to four weeks ahead. Amongst the drivers examined, the MJO has the largest impact  
19 on the forecast skill of rainfall modes within the ECMWF model. If MJO-related variability is reliably represented, the  
20 ECMWF model is more skilful at predicting the main modes of weekly rainfall variability over the region. Our findings can  
21 support model developments and enhance anticipatory planning efforts in several sectors, such as agriculture, food security,  
22 and energy.

AQ1 AQ2

23 **Keywords** Eastern Africa Short Rains · Empirical Orthogonal Function Analysis · Madden–Julian Oscillation · El Niño–  
24 Southern Oscillation · Indian Ocean Dipole · Sub-seasonal Prediction Skill

## 25 1 Introduction

26 Rainfall variations in Eastern Africa, which includes the  
27 countries of Burundi, Djibouti, Eritrea, Ethiopia, Kenya,  
28 Rwanda, Somalia, Sudan, South Sudan, Tanzania, and  
29 Uganda (Fig. 1), with a total population of 457 million peo-  
30 ple (Palmer et al. 2023), may substantially impact several  
31 crucial activities in the region, in sectors such as agriculture,  
32 food security, and energy (Funk et al. 2008; Anande and  
33 Luhunga 2019; Chang'a et al. 2020; FSNAU 2022; Palmer

34 et al. 2023). Thus, there has been an increasing interest in  
35 understanding what controls Eastern Africa rainfall vari-  
36 ability (Ogallo et al. 1988; Ogallo 1989; Indeje et al. 2000;  
37 Black et al. 2003; Schreck and Semazzi 2004; Bowden and  
38 Semazzi 2007; Berhane and Zaitchik 2014; Gamoyo et al.  
39 2015; Nicholson 2017; Wenhaji Ndomeni et al. 2018; Kol-  
40 stad and MacLeod 2022; Maybee et al. 2022; among others).

41 Specifically, significant variations in Eastern Africa rain-  
42 fall occur throughout the October–November–December  
43 (OND) short rains (Nicholson 2017; Palmer et al. 2023),  
44 showing, in particular, large interannual/seasonal variabil-  
45 ity (Camberlin and Wairoto 1997; Camberlin et al. 2009).  
46 Previous studies have investigated the sources of seasonal  
47 short rains variability, mainly indicating associations with  
48 El Niño–Southern Oscillation (ENSO; Nicholson and Kim  
49 1997; Schreck and Semazzi 2004; Bowden and Semazzi  
50 2007; Hoell et al. 2014; MacLeod et al. 2021; Kolstad and

A1 Felipe M. de Andrade  
A2 felipestratus@gmail.com

A3 <sup>1</sup> National Centre for Atmospheric Science and Department  
A4 of Meteorology, University of Reading, Reading, UK

A5 <sup>2</sup> National Institute for Space Research, Cachoeira Paulista, SP,  
A6 Brazil

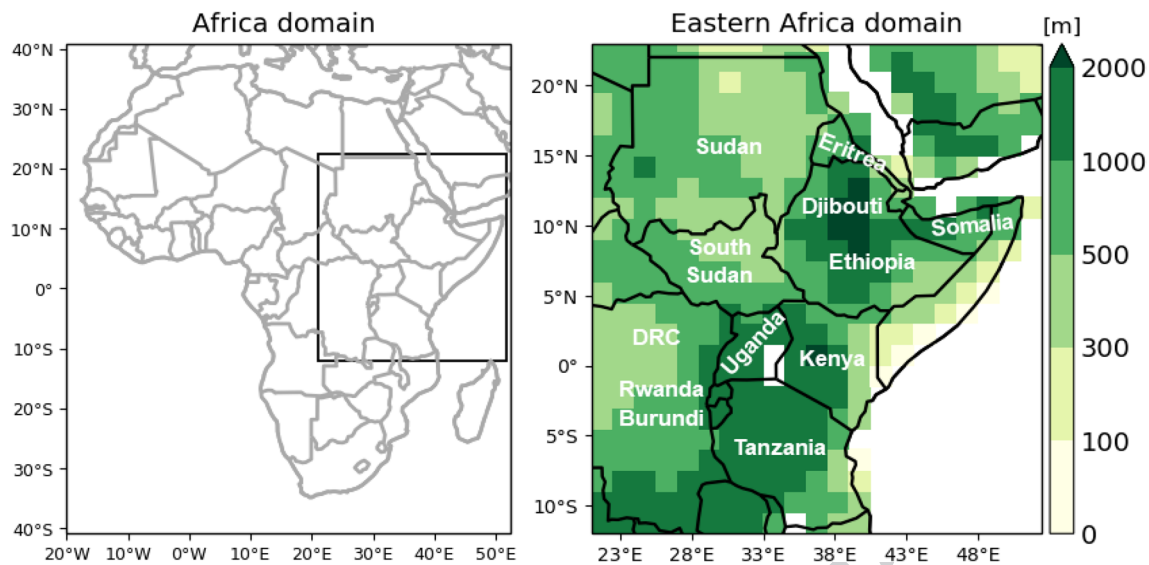


**Fig. 1** Africa domain in the left panel with a black box indicating the Eastern Africa domain ( $12^{\circ}\text{S}$ - $23^{\circ}\text{N}$ ,  $21^{\circ}$ - $52^{\circ}\text{E}$ ) magnified in the right panel. Burundi, Djibouti, Eritrea, Ethiopia, Kenya, Rwanda, Somalia, Sudan, South Sudan, Tanzania, and Uganda are the 11 countries

comprising the Eastern Africa domain. DRC stands for Democratic Republic of the Congo. Topography (shaded) in the right panel is shown in metres (m) and sourced from ERA5 reanalysis (Hersbach et al. 2020)

MacLeod 2022) and the Indian Ocean Dipole (IOD; Black et al. 2003; Behera et al. 2005; Nicholson 2015; Hiron and Turner 2018; Bahaga et al. 2019; Kolstad and MacLeod 2022). Strong co-variability exists between ENSO and the IOD (Nicholson 2015; Zhang et al. 2015), with the latter typically having more influence than the former on the short rains owing to its modulation of local zonal circulation (Goddard and Graham 1999; Bergonzini et al. 2004; Nicholson 2015; Zhao and Cook 2021). A weaker-than-normal zonal circulation over the Indian Ocean is related to positive sea surface temperature (SST) anomalies in the west and negative SST anomalies in the east, leading to enhanced rainfall in Eastern Africa (Black et al. 2003; Behera et al. 2005; Ummenhofer et al. 2009). The opposite SST pattern strengthens the zonal circulation over the Indian Ocean (Jiang et al. 2021; Zhao and Cook 2021), favouring reduced rainfall in Eastern Africa (Black et al. 2003; Behera et al. 2005). The most recent noticeable impact of an IOD event occurred in Eastern Africa's 2019 short rains and was associated with substantially above-average rains that forced hundreds of thousands of people to flee their homes and caused crop and livestock losses in the areas severely affected (Wainwright et al. 2021).

In addition to seasonal rainfall variability, sub-seasonal short rains anomalies (i.e., wet and dry spells within the rainy season that extend longer than the synoptic timescale) have also been identified (Camberlin and Wairoto 1997; Mutai and Ward 2000; Pohl and Camberlin 2006a; b; Zaitchik 2017). Such sub-seasonal rainfall variations are mainly related to the influence of the Madden-Julian

Oscillation (MJO) over Eastern Africa, with significant phasing dependence (Pohl and Camberlin 2006a; b; Omeny et al. 2008; Berhane and Zaitchik 2014; Hogan et al. 2015). In general, rainfall increases (reduces) in most of Eastern Africa when the MJO-enhanced convective core is over the tropical Indian Ocean (Western Pacific) (Omeny et al. 2008; Hogan et al. 2015), as indicated by phases 2 and 3 (6 and 7) of the Real-Time Multivariate MJO index (RMM; Wheeler and Hendon 2004).

While seasonal predictions of short rains variability show great accuracy several months ahead of a season in association with ENSO and IOD modulation (Bahaga et al. 2015; MacLeod 2019; Walker et al. 2019), sub-seasonal prediction skill of short rains variability over a few weeks ahead remains relatively modest (Vigaud et al. 2018; 2019; de Andrade et al. 2021; Kolstad et al. 2021), with correlations rarely above 0.4 after two weeks lead time (de Andrade et al. 2021). As a result, linearly corrected forecasts have emerged and, to some extent, skill improvements have been linked to potential drivers of sub-seasonal to seasonal predictability such as the MJO, ENSO, and the IOD (Vigaud et al. 2018; de Andrade et al. 2021; Kolstad et al. 2021). Nevertheless, improving our understanding of sub-seasonal short rains variability, particularly the underlying drivers that modulate the local rainfall impacts, is essential to better predicting and anticipating sub-seasonal rainfall anomalies in Eastern Africa.

Here, an in-depth investigation of sub-seasonal variability and prediction skill of short rains is performed by examining its leading weekly rainfall modes rather than the

111 commonly assessed weekly rainfall anomalies within the  
 112 season (Vigaud et al. 2019; de Andrade et al. 2021). This  
 113 approach allows us to evaluate distinct weekly rainfall vari-  
 114 ability patterns accounting for the largest portion of the total  
 115 variance in the sub-seasonal rainfall anomalies. While this  
 116 approach has been applied in a small number of studies at  
 117 pentad and seasonal timescales (Schreck and Semazzi 2004;  
 118 Bowden and Semazzi 2007; Wenhaji Ndomeni et al. 2018;  
 119 Kolstad and MacLeod 2022), evidence is lacking for further  
 120 assessing the leading modes of Eastern Africa short rains  
 121 variability at weekly timescales, along with their represen-  
 122 tation within dynamical models, sources of predictability,  
 123 and prediction skill. Given that, the following questions are  
 124 addressed:

125 What are the leading modes of weekly Eastern Africa  
 126 short rains variability and their relationships with poten-  
 127 tial climate drivers?

128 What is the current ability of the models to capture and  
 129 predict the leading rainfall modes at different weekly lead  
 130 times?

131 What is the contribution of climate drivers to the sub-  
 132 seasonal predictive skill of the leading rainfall modes?

133 Providing answers to the questions above would help  
 134 advance the scientific understanding, support model devel-  
 135 opments, and contribute to assisting sectors in taking  
 136 preparedness measures that reduce or avoid the effects of  
 137 high-impact weather conditions on people's lives and live-  
 138 lihoods in Eastern Africa (Hirons et al. 2021; Gudoshava  
 139 et al. 2022). The paper is organised as follows: Section 2  
 140 presents the datasets and methods used, Section 3 describes  
 141 the results from this study, and Section 4 summarises key  
 142 findings and provides conclusions.

## 144 2 Methodology

### 144 2.1 Observational analysis

145 Rainfall data sourced from the Tropical Applications of  
 146 Meteorology using SATellite and ground-based observa-  
 147 tions (TAMSAT; Maidment et al. 2014; 2017) version 3.1  
 148 were used to investigate observed sub-seasonal Eastern  
 149 Africa short rains variability. Land-only TAMSAT rain-  
 150 fall estimates are derived from rain gauge measurements  
 151 used for calibration and thermal infrared satellite imagery  
 152 (Maidment et al. 2017). Here, the spatial resolution of  
 153 daily TAMSAT data was linearly interpolated (using bi-  
 154 linear interpolation) from the regular  $0.0375^\circ \times 0.0375^\circ$   
 155 grid to  $1.5^\circ \times 1.5^\circ$  to facilitate the comparison with mod-  
 156 elled outputs, as shown later. Although TAMSAT produces  
 157 rainfall estimates from 1983 to the present, we focused

158 on the 1999–2016 period to match all datasets temporal  
 159 resolution analysed here. Weekly data were obtained by  
 160 averaging seven consecutive days without overlapping  
 161 from October 1st to December 24th, totalling 13 weeks  
 162 within the short rains season. This produces a sample  
 163 size of 234 weeks between 1999 and 2016 (13 weeks over  
 164 18 years). Weekly rainfall anomalies were computed by  
 165 subtracting the corresponding 1999–2016 long-term mean  
 166 from the total field.

167 Given the known uncertainty in rainfall observations in  
 168 the region (Sylla et al. 2013), three other observational data-  
 169 sets were assessed to examine how sensitive the results are to  
 170 selecting the observational reference, following the method  
 171 described to obtain weekly TAMSAT rainfall anomalies.  
 172 The additional datasets are the land-only Climate Hazards  
 173 Group Infrared Precipitation with Stations (CHIRPS; Funk  
 174 et al. 2015), the Global Precipitation Climatology Project  
 175 (GPCP; Huffman et al. 2001) version 1.3, and the Tropi-  
 176 cal Rainfall Measuring Mission (TRMM) Multi-Satellite  
 177 Precipitation Analysis 3B42 (Huffman et al. 2007). These  
 178 datasets were chosen because they are also frequently used  
 179 satellite-derived products to study rainfall variability in East-  
 180 ern Africa (Dinku et al. 2007; 2011; Kimani et al. 2017;  
 181 Agete et al. 2022; Palmer et al. 2023).

182 Empirical orthogonal function (EOF; Wilks 2006)  
 183 analysis was performed on all the observational datasets to  
 184 identify the leading modes of weekly rainfall variability in  
 185 the Eastern Africa domain (Fig. 1). The EOF analysis used  
 186 GPCP and TRMM data with masking over oceanic regions  
 187 to consider all datasets with land-only grid point informa-  
 188 tion. The eigenvalues and eigenvectors of an anomaly covar-  
 189 iance matrix of a field were computed to extract the EOF  
 190 modes. Since the EOF analysis does not consist of physi-  
 191 cal assumptions, a field is separated into mathematically  
 192 orthogonal modes, which occasionally can be translated into  
 193 physical structures (Hannachi et al. 2007). The eigenvalues  
 194 are used to express the percentage of variance explained  
 195 by each EOF mode. Nevertheless, the eigenvalues may not  
 196 always be distinguishable owing to sampling issues. The  
 197 North's rule of thumb was used to overcome this constraint  
 198 by evaluating if a particular eigenvalue is distinct from its  
 199 nearest neighbour and indicating when a sampling error  
 200 is expected to be significant (North et al. 1982). Rainfall  
 201 anomalies were projected onto the generated eigenvectors  
 202 to produce normalised time series, or principal components  
 203 (PCs), associated with each EOF mode.

204 To investigate possible associations between the domi-  
 205 nant modes of weekly Eastern Africa short rains vari-  
 206 ability and potential drivers of sub-seasonal rainfall vari-  
 207 ations, we calculated climate indices frequently used as  
 208 indicators of MJO, ENSO, and IOD activity. These are the  
 209 RMM daily index (Wheeler and Hendon 2004), the Niño  
 210 3.4 (hereafter referred to as N3.4) index (Trenberth and

211 Stepaniak 2001) and the Dipole Mode Index (DMI; Saji  
 212 et al. 1999), respectively.

213 The European Centre for Medium-Range Weather  
 214 Forecasts (ECMWF) data store provided the RMM  
 215 components (i.e., RMM1 and RMM2) calculated as  
 216 in (Vitart 2017). The RMM components illustrate dif-  
 217 ferent phases of the MJO cycle (Wheeler and Hendon  
 218 2004), with RMM1 (RMM2) representing MJO convec-  
 219 tive anomalies over the Maritime Continent and Western  
 220 Hemisphere (tropical Indian Ocean and western Pacific).  
 221 These indices are the two leading PCs extracted from  
 222 an EOF analysis, which combines daily zonal upper-  
 223 (200 hPa) and lower- (850 hPa) wind and outgoing long-  
 224 wave radiation anomalies in the tropics after subtracting  
 225 the low-frequency variability associated with ENSO (as  
 226 in Wheeler and Hendon 2004). Weekly RMM compo-  
 227 nents were determined using the same approach applied to  
 228 obtain weekly rainfall totals. SST anomalies in the N3.4  
 229 region (5°S–5°N, 120°–170°W) were averaged to pro-  
 230 duce the N3.4 index, whereas the DMI index was deter-  
 231 mined by the difference between SST anomalies in the  
 232 western (10°S–10°N, 50°–70°E) and eastern (10°S–0°,  
 233 90°–110°E) tropical Indian Ocean. SST data were sourced  
 234 from the daily optimum interpolation SST version 2 of  
 235 the National Oceanic and Atmospheric Administration  
 236 (NOAA; Reynolds et al. 2007). The same technique  
 237 applied to find weekly rainfall anomalies was employed  
 238 to obtain weekly SST anomalies, which were used to cal-  
 239 culate N3.4 and DMI indices. The respective standard  
 240 deviations were utilised to normalise weekly SST anom-  
 241 ality indices. Additionally, considering that ENSO and IOD  
 242 may have strong associations during the boreal autumn  
 243 (Nicholson 2015; Zhang et al. 2015), we removed from  
 244 N3.4 and DMI indices their variability associated with  
 245 DMI and N3.4 indices (hereafter referred to as N3.4\*  
 246 and DMI\* indices), respectively. This was performed by  
 247 first computing a simple linear regression (Allen 1997)  
 248 between the response and explanatory variables, then sub-  
 249 tracting the corresponding co-variability from N3.4 and  
 250 DMI indices.

251 Pearson's correlation (Wilks 2006) was computed to  
 252 indicate linear associations between the leading TAM-  
 253 SAT PCs and drivers' indices, in addition to showing  
 254 the strength of the linear relationship between the PCs  
 255 derived from observational datasets. The magnitude of  
 256 the correlation was determined by its absolute value (or  
 257 modulus). Therefore, the higher the absolute correlation,  
 258 the stronger the association. A two-sided Student's t-test  
 259 with a 95% significance level was used to examine the  
 260 statistical robustness of correlations distinct from zero  
 261 (Wilks 2006). Based on lag-1 autocorrelation, the effec-  
 262 tive sample size was estimated as in Livezey and Chen  
 263 (1983).

## 2.2 Hindcast assessment

264 The ability of dynamical models to capture and predict  
 265 the leading modes of sub-seasonal Eastern Africa short  
 266 rains variability was evaluated using hindcasts from  
 267 ECMWF, the National Centers for Environmental Prediction  
 268 (NCEP), and the UK Met Office (UKMO) models.  
 269 Using these models allows us, in particular, to expand  
 270 the hindcast assessment conducted by de Andrade et al.  
 271 (2021), contributing to enhancing the knowledge of  
 272 sub-seasonal rainfall forecast quality in Eastern Africa.  
 273 Rainfall hindcasts were obtained from two sub-seasonal  
 274 forecasting databases: the Subseasonal to Seasonal (S2S)  
 275 prediction project (Vitart et al. 2017) for ECMWF and  
 276 UKMO models, and the Subseasonal Experiment (SubX;  
 277 Pegion et al. 2019) for the NCEP model. The SubX data-  
 278 base was used for NCEP to allow a longer time frame  
 279 (i.e., 1999–2016) than what is provided in the S2S data-  
 280 base (i.e., 1999–2010). ECMWF and UKMO hindcasts  
 281 were sourced at the regular  $1.5^\circ \times 1.5^\circ$  spatial resolu-  
 282 tion, whereas the NCEP grid was reduced from  $1^\circ \times 1^\circ$  to  
 283  $1.5^\circ \times 1.5^\circ$  using bi-linear interpolation. As in de Andrade  
 284 et al. (2021), four start dates per month, based on weekly  
 285 UKMO initialisations, were evaluated for each model,  
 286 accounting for the closest start dates for some non-matching  
 287 ECMWF initialisations. Moreover, three perturbed  
 288 members, drawn from 1-day lag after initialisations, were  
 289 added to the NCEP ensemble size to achieve an accurate  
 290 intercomparison between models while considering the  
 291 same ensemble size (i.e., at least 7 ensemble members).  
 292 The amount of weekly rainfall was defined by averaging  
 293 the following daily forecast lead times falling within the  
 294 short rains season: days 5–11 (Week 1), 12–18 (Week 2),  
 295 19–25 (Week 3), and 26–32 (Week 4). This implied that  
 296 a few initialisations in September and December were  
 297 respectively included and removed when evaluating tar-  
 298 gets at Weeks 2–4 leads. The ensemble mean climatology,  
 299 calculated considering a leave-one-out cross-validation  
 300 approach (Wilks 2006), was subtracted from the ensemble  
 301 mean totals to obtain the corresponding anomalies over  
 302 the 1999–2016 period. The procedure was carried out  
 303 depending on the start date and lead time. An equivalent  
 304 method was used to determine observed rainfall anomalies  
 305 in Weeks 1–4.

306 The leading PCs of modelled rainfall variability at Weeks  
 307 1–4 were calculated by projecting land-only model anom-  
 308 alies onto the observed rainfall eigenvectors determined  
 309 in Section 2.1. By regressing the derived PCs and model  
 310 anomalies, it yielded the corresponding modelled regressed  
 311 spatial modes (RSMs). Observed PCs and associated RSMs  
 312 at Weeks 1–4 were obtained considering the same approach  
 313 used to identify the dominant rainfall modes within models.  
 314 To extract modelled and observed spatiotemporal modes

316 for each lead time, we utilised samples with 180 (i.e., 10  
 317 start dates over 18 years) weekly hindcast and observation  
 318 anomalies, respectively.

319 The ability of the model to capture the RSMs was evaluated  
 320 by computing spatial correlation (i.e., Pearson's correlation  
 321 was examined in two spatial dimensions considering an  
 322 area-average weighted with latitude) and the region-averaged  
 323 absolute difference (or modulus of the difference) between  
 324 modelled and observed RSMs. Additionally, the ability of  
 325 the model to predict the PCs was assessed by computing  
 326 Pearson's correlation and root mean squared error (RMSE;  
 327 Wilks 2006) between modelled and observed PCs. Correla-  
 328 tions were computed to assess model phase errors, with  
 329 values equal to one indicating the strongest linear associa-  
 330 tions between observations and model data. On the other  
 331 hand, model amplitude errors were assessed using RMSE  
 332 and absolute difference, with values equal to zero indicat-  
 333 ing the best model accuracy. The statistical significance of  
 334 the correlations was examined as described in Section 2.1.

### 335 2.3 Drivers of model skill

336 The contribution of climate drivers in modulating the  
 337 ECMWF model skill at predicting the main modes of weekly  
 338 Eastern Africa short rains variability was investigated  
 339 employing a similar methodology as the one described in  
 340 de Andrade et al. (2021). The method assesses the ECMWF  
 341 model skill after replacing the modelled driver-related  
 342 rainfall variability with the corresponding observed driver-  
 343 related response in the hindcasts. Observed and modelled  
 344 driver-related rainfall variabilities are derived from the  
 345 corresponding linear regression between rainfall anomalies and  
 346 climate indices representing MJO, ENSO, and IOD varia-  
 347 tions. Here, RMM, N3.4, and DMI indices were respectively  
 348 used to characterise MJO, ENSO, and IOD activity as in de  
 349 Andrade et al. (2021). Daily RMM components for each  
 350 model ensemble member were sourced from the ECMWF  
 351 data store, allowing the computation of the 7-member  
 352 ensemble mean for RMM1 and RMM2 indices at Weeks  
 353 1–4. Furthermore, daily SST hindcasts from the S2S data-  
 354 base were used to obtain the 7-member ensemble mean of  
 355 weekly SST anomalies, following the procedures adopted to  
 356 obtain weekly rainfall anomalies in Section 2.2. ENSO and  
 357 IOD indices at Weeks 1–4 were computed as in Sect. 2.1,  
 358 with their co-variability also removed from modelled N3.4\*  
 359 and DMI for producing modelled N3.4\* and DMI\* indices.  
 360 Both indices were normalised by the corresponding stand-  
 361 ard deviation depending on the initialisation and lead time.  
 362 Suitable datasets specified in Sect. 2.1 were used to produce  
 363 the observed RMM1, RMM2, N3.4\*, and DMI\* indices in  
 364 Weeks 1–4.

365 Next, we performed a simple linear regression analysis  
 366 between weekly rainfall anomalies and MJO, ENSO, and

367 IOD indices. We subtracted from both observed and mod-  
 368 modelled rainfall anomalies the corresponding variations in rain-  
 369 fall that were linearly associated with each driver. Rainfall  
 370 anomalies without the presence of drivers' signals were used  
 371 to calculate observed and modelled PCs at Weeks 1–4 as in  
 372 Section 2.2. After removing driver-related rainfall variability  
 373 from modelled rainfall anomalies, the impact on the model  
 374 skill was also investigated by adding observed regression  
 375 patterns to hindcasts, producing a new set of model rain-  
 376 fall anomalies utilised to obtain corrected PCs. The model  
 377 skill was evaluated by measuring the percentage change in  
 378 Pearson's correlation between the resulting observed and  
 379 modelled PCs according to (1):

$$( \hat{R} - R ) / R * 100 \quad (1) \quad 380$$

381 Where R is the correlation computed without modifying any  
 382 driver-related signals in rainfall anomalies, and  $\hat{R}$  is the cor-  
 383 relation after removing or adding particular driver-related  
 384 signals in rainfall anomalies. Positive (Negative) values of  
 385 (1) denote strengthening (weakening) in the association  
 386 between observed and modelled PCs, indicating, therefore,  
 387 improvements (degradations) in the model skill.

## 389 3 Results

390 The results are organised into three sections, which system-  
 391 atically respond to the questions presented in Section 1. The  
 392 first Section (3.1) identifies and compares the leading modes  
 393 of sub-seasonal Eastern Africa short rains variability from  
 394 distinct observational datasets, and shows how these modes  
 395 relate to specific climate drivers. The second Section (3.2)  
 396 presents a hindcast evaluation for investigating the ability of  
 397 the model to capture and predict the leading rainfall modes  
 398 at forecast horizons from one to four weeks into the future.  
 399 The third Section (3.3) furthers this evaluation to consider  
 400 how the model quality is related to the potential sources of  
 401 sub-seasonal climate variability.

### 3.1 The leading EOF modes and their associations 402 with climate drivers

403 Figure 2 shows weekly TAMSAT rainfall climatology, the  
 404 standard deviation of associated anomalies, and the corre-  
 405 sponding EOF analysis for Eastern Africa rainfall anomalies  
 406 during the short rains season from October to December.  
 407 The highest climatological rainfall totals are located over  
 408 elevated topography in the western sector of Eastern Africa,  
 409 covering parts of Burundi, Rwanda, South Sudan, Tanzania,  
 410 Uganda, and the central-eastern Democratic Republic of the  
 411 Congo (DRC; Figs. 1, 2a). In contrast, the highest rainfall  
 412 variability appears in the southeastern sector of Eastern  
 413 Africa.

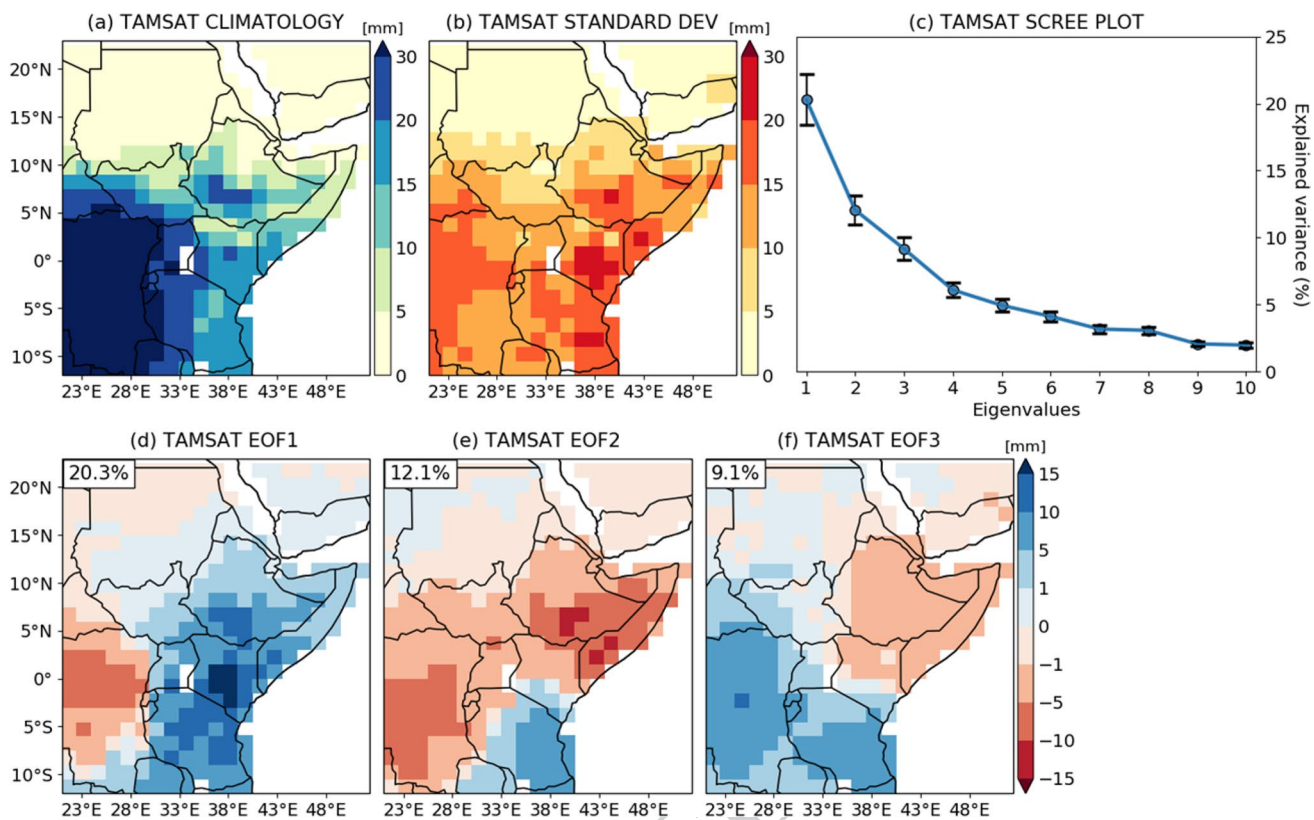


**Fig. 2** Weekly TAMSAT accumulated rainfall (a) climatology and (b) standard deviation for Eastern Africa short rains season (OND). (c) Scree plot showing the corresponding explained variance in percentage (%) for the first ten eigenvalues of the EOF analysis from weekly TAMSAT rainfall anomalies. Sample errors are indicated by the error

bars in (c) according to the North's rule of thumb. The first three spatial EOF modes (or eigenvectors) for weekly TAMSAT rainfall accumulation anomalies are respectively displayed in (d), (e), and (f), with their explained variance in percentage (%) shown in the top-left corner. Rainfall accumulations are in millimetres (mm)

414 Africa, including the highlands of Ethiopia and Kenya, as  
 415 well as coastal regions in Somalia and Tanzania (Figs. 1,  
 416 2b). The first three EOF modes for TAMSAT show spatial  
 417 structures that influence varying rainfall levels in most  
 418 Eastern Africa countries and, when combined, account for  
 419 41.5% of the total variance (Figs. 2d, e, f). According to the  
 420 criteria of North et al. (1982), these dominant modes are  
 421 distinguished from each other and well separated from the  
 422 degenerate set of higher EOFs (Fig. 2c).

423 The first leading mode (EOF1) is characterised by a mon-  
 424 opole-like rainfall pattern with the largest positive rainfall  
 425 anomalies affecting southern Ethiopia, Kenya, and north-  
 426 ern Tanzania (Fig. 2d). The second (EOF2) and the third  
 427 (EOF3) modes show a dipole-like rainfall pattern with pos-  
 428 itive anomalies in Tanzania and negative anomalies in the  
 429 northeastern portion of Eastern Africa, which covers Djib-  
 430 outi, Eritrea, Ethiopia, and Somalia (Figs. 2e, f). EOF2 and  
 431 EOF3 have similar spatial characteristics in the eastern part  
 432 of the domain and coastal regions, whereas opposite signals  
 433 are seen further inland (Figs. 2e, f). Although using other  
 434 datasets, periods, and domains, the EOF modes found here  
 435 generally correspond well with the main modes of seasonal

436 and pentad Eastern Africa rainfall variability identified in  
 437 previous studies (Schreck and Semazzi 2004; Bowden and  
 438 Semazzi 2007; Wenhaji Ndomeni et al. 2018; Kolstad and  
 439 MacLeod 2022).

440 To investigate sources of sub-seasonal Eastern Africa  
 441 short rains variability, Fig. 3 presents the correlations  
 442 between potential climate drivers' indices and the first three  
 443 TAMSAT PCs. RMM1 exhibits strong significant connec-  
 444 tions with PC2 and PC3, whereas

445 RMM2 shows high significant co-variability linked to  
 446 PC1 (Fig. 3a). Despite N3.4 and DMI showing significant  
 447 correlations with PC1, as also found in previous studies  
 448 (Schreck and Semazzi 2004; Bowden and Semazzi 2007;  
 449 Kolstad and MacLeod 2022), it is worth pointing out that  
 450 for N3.4, removing the signal associated with DMI makes  
 451 the association insignificant (compare the correlations  
 452 when considering the ENSO index as N3.4 (darkest blue  
 453 bar) and N3.4\* (lightest blue bar) in Fig. 3a), whereas  
 454 removing the N3.4 signal from DMI does weaken the  
 455 correlation with PC1 but it is still significant (compare  
 456 the correlations when considering the DMI index as DMI  
 457 (darkest red bar) and DMI\* (lightest red bar) in Fig. 3a).

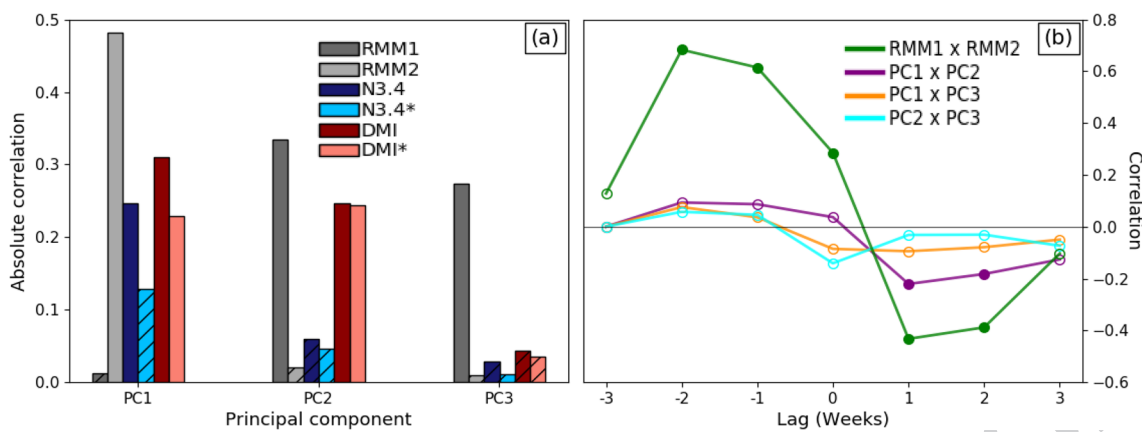


**Fig. 3** (a) Absolute Pearson's correlation between weekly TAMSAT PC1 to PC3 and observed weekly drivers' indices represented by RMM1, RMM2, N3.4, and DMI. N3.4\* (DMI\*) indicates that the DMI (N3.4) signal has been removed from the N3.4 (DMI) index. (b) Lagged correlations between RMM1 and RMM2, as well as between

the leading TAMSAT PCs. A positive (negative) lag indicates RMM1 leads (lags) RMM2, for instance. Hatching over the bars in (a) and open circle markers in (b) denote correlation coefficients that are not statistically significant at the 95% confidence level according to a two-tailed Student's t-test

458 For PC2, the correlations indicate that the MJO and IOD  
459 have significant associations with the dipole-like rainfall  
460 variability in the region. In contrast, there are no sig-  
461 nificant associations between ENSO and PC2 (Fig. 3a).  
462 Unlike PC1 and PC2, PC3 does not significantly correlate  
463 with SST indices, which mainly emphasises its rela-  
464 tionship with the MJO (Fig. 3a).

465 The climate drivers' associations with TAMSAT PC1  
466 and PC2 (Fig. 3a), along with the corresponding TAMSAT  
467 spatial modes shown in Fig. 2, generally are consistent with  
468 the regression patterns that de Andrade et al. (2021) found  
469 when relating similar drivers' indices to weekly GPCP  
470 rainfall anomalies. That is, EOF1 (Fig. 2d) compares quite  
471 strongly to the September–October–November RMM2- and  
472 DMI-related rainfall patterns shown in de Andrade et al.  
473 (2021) (see SON in their Fig. 9), whereas EOF2 (Fig. 2e)  
474 reasonably matches with the corresponding SON RMM1-  
475 related rainfall pattern. Moreover, December–January–Fe-  
476 bruary N3.4- and RMM1-related rainfall patterns shown in de  
477 Andrade et al. (2021) (see DJF in their Fig. 9) also indicate  
478 consistent signals with TAMSAT EOF1 (Fig. 2d) and EOF2  
479 (Fig. 2e), respectively. All these characteristics corroborate  
480 with GPCP EOF1 and EOF2, as shown later in Fig. 5.

481 To specifically deepen understanding of the MJO-related  
482 Eastern Africa rainfall variability, Fig. 3b shows the lagged  
483 correlation between RMM components, as well as between  
484 TAMSAT PC1, PC2, and PC3. Significant correlations for  
485 PC1 and PC2 are identified at 1–2-week lags, showing that  
486 PC1 generally leads PC2 by a few weeks (Fig. 3b; purple line).  
487 This agrees with the MJO cycle, which also indicates  
488 that RMM1 and RMM2 occur sequentially with significant  
489 correlations at 1–2-week lags (Fig. 3b; green line). How-  
490 ever, the correlations between PC1 and PC3 or PC2 and

491 PC3 are not significant across all lags (Fig. 3b; orange and  
492 blue lines).

493 The results discussed so far have been carried out using  
494 TAMSAT data. To examine the sensitivity of weekly rainfall  
495 to the choice of the observational dataset, Fig. 4 displays the  
496 climatology and standard deviation for CHIRPS (Figs. 4a,  
497 d), GPCP (Figs. 4b, e), and TRMM (Figs. 4c, f) data during  
498 OND.

499 All datasets show the highest climatological rainfall  
500 totals in the western sector of the domain (Figs. 4a, b, c)  
501 and the highest rainfall deviations in the southeastern sector  
502 of Eastern Africa (Figs. 4d, e, f), overall corroborating with  
503 TAMSAT data (Figs. 2a, b). Nevertheless, higher (lower) cli-  
504 matological rainfall totals are seen over Kenya for CHIRPS  
505 and TRMM (GPCP) data (compare Fig. 2a with Figs. 4a,  
506 c (Fig. 4b)), whereas higher (lower) rainfall variations are  
507 found further inland for GPCP and TRMM (CHIRPS) data  
508 (compare Fig. 2b with Figs. 4e, f (Fig. 4d)). Despite these  
509 minor differences in the rainfall data, there is considerable  
510 agreement in the weekly evolution of the region-averaged  
511 rainfall anomalies throughout the short rains when compar-  
512 ing all datasets (Online Resource 1—Fig. 1). These find-  
513 ings, therefore, contribute to increasing the reliability of the  
514 observed rainfall variability in the region and its related EOF  
515 analysis, as shown below.

516 Figure 5 displays the first three spatial EOF modes and  
517 scree plots for CHIRPS, GPCP, and TRMM rainfall anom-  
518 alies. The combined explained variance of EOF1, EOF2,  
519 and EOF3 is 42.1% for CHIRPS (Figs. 5a, b, c), 45.4% for  
520 GPCP (Figs. 5e, f, g), and 34.4% for TRMM (Figs. 5i, j, k).  
521 Thus, the sum of the explained variance of TRMM is lower  
522 than that of CHIRPS or GPCP when compared to TAMSAT  
523 (41.5%; Figs. 2d, e, f).

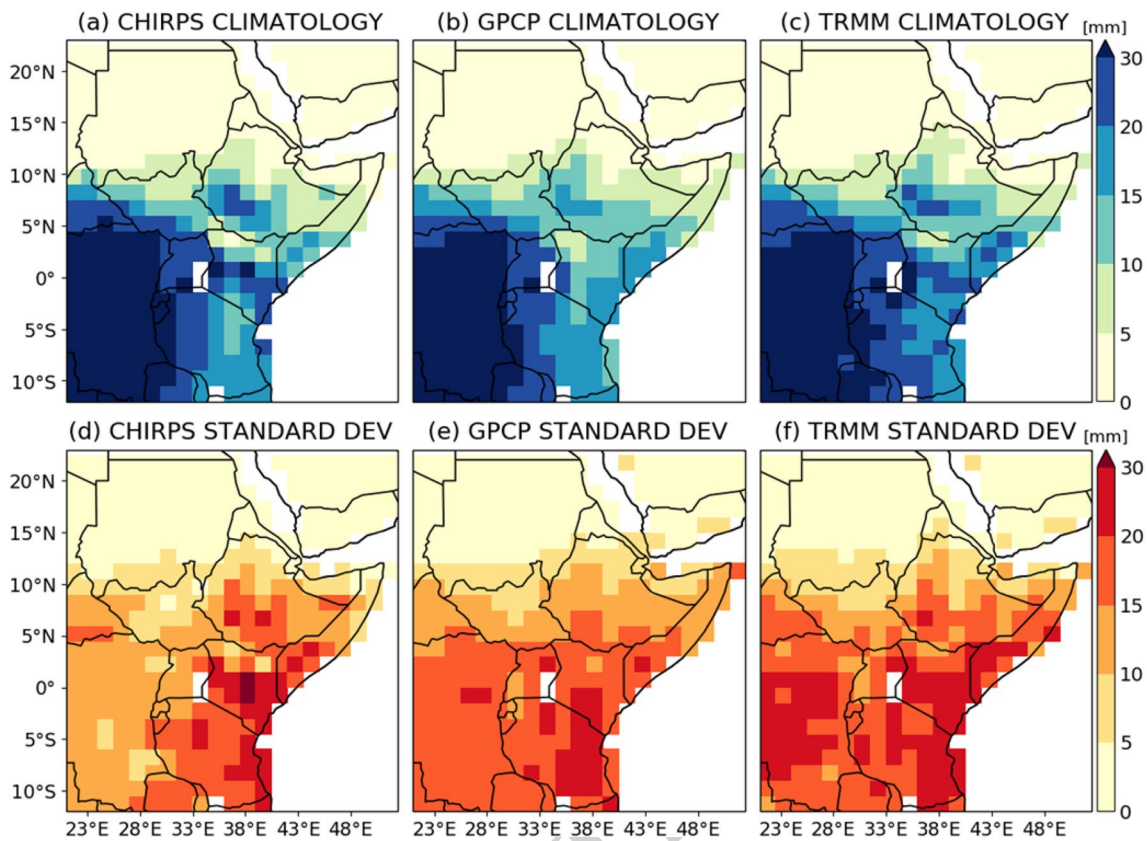


**Fig. 4** Weekly accumulated rainfall (upper panel) climatology and (lower panel) standard deviation for (a, d) CHIRPS, (b, e) GPCP, and (c, f) TRMM datasets during the Eastern Africa short rains season (OND). Rainfall accumulations are in millimetres (mm)

The spatial patterns associated with EOF1 and EOF2 from the additional datasets (CHIRPS, GPCP, and TRMM) are similar to the ones found for TAMSAT, i.e., a monopole-like rainfall pattern for EOF1 (compare Fig. 2d with Figs. 5a, e, i) and a dipole-like rainfall pattern for EOF2 (compare Fig. 2e with Figs. 5b, f, j). For EOF3, however, there are discrepancies when comparing its spatial pattern among the datasets. While GPCP shows positive rainfall anomalies in Tanzania and negative rainfall anomalies in the northeastern sector of Eastern Africa in agreement with TAMSAT (compare Fig. 2f with Fig. 5g), CHIRPS and TRMM exhibit rainfall patterns that differ from TAMSAT (compare Fig. 2f with Figs. 5c, k). The uncertainty in representing EOF3 in the observations is also seen through the scree plots, showing distinct sample errors and how separated this mode is from EOF2 and higher EOF modes, depending on the dataset (Figs. 5d, h, l).

To further assess the representation of the leading EOF modes within CHIRPS, GPCP, and TRMM datasets, Fig. 6 shows the association between the first three TAMSAT PCs and the first ten PCs (PC1 to PC10) derived from the EOF analysis using CHIRPS, GPCP, and TRMM rainfall anomalies. The highest correlation coefficients indicate that

TAMSAT PC1 and PC2 are adequately represented across all datasets, particularly in CHIRPS data (Figs. 6a, b). However, Fig. 6c shows there is some sensitivity to the selection of the reference data when performing an EOF analysis of weekly rainfall anomalies for Eastern Africa short rains, specifically that TAMSAT PC3 properties are not well represented by other datasets, notably CHIRPS and TRMM as also seen in the spatial patterns (compare Fig. 2f with Figs. 5c, k). In fact, CHIRPS can reasonably represent the temporal variability associated with EOF3, though it is captured by the fourth EOF mode (Fig. 6c).

The following two sections only address a model evaluation for the first two EOF modes (EOF1 and EOF2) owing to the inconsistency in representing EOF3 across the datasets (Figs. 2, 5, 6). Moreover, the results for the TAMSAT dataset are exclusively used when assessing model hindcasts, as the sensitivity to the reference data selection is minimal for the two leading rainfall modes (Figs. 2, 5, 6).

### 3.2 Model evaluation

Figures 7 and 8 show the model capability to capture the first (RSM1) and the second (RSM2) RSMs at lead times

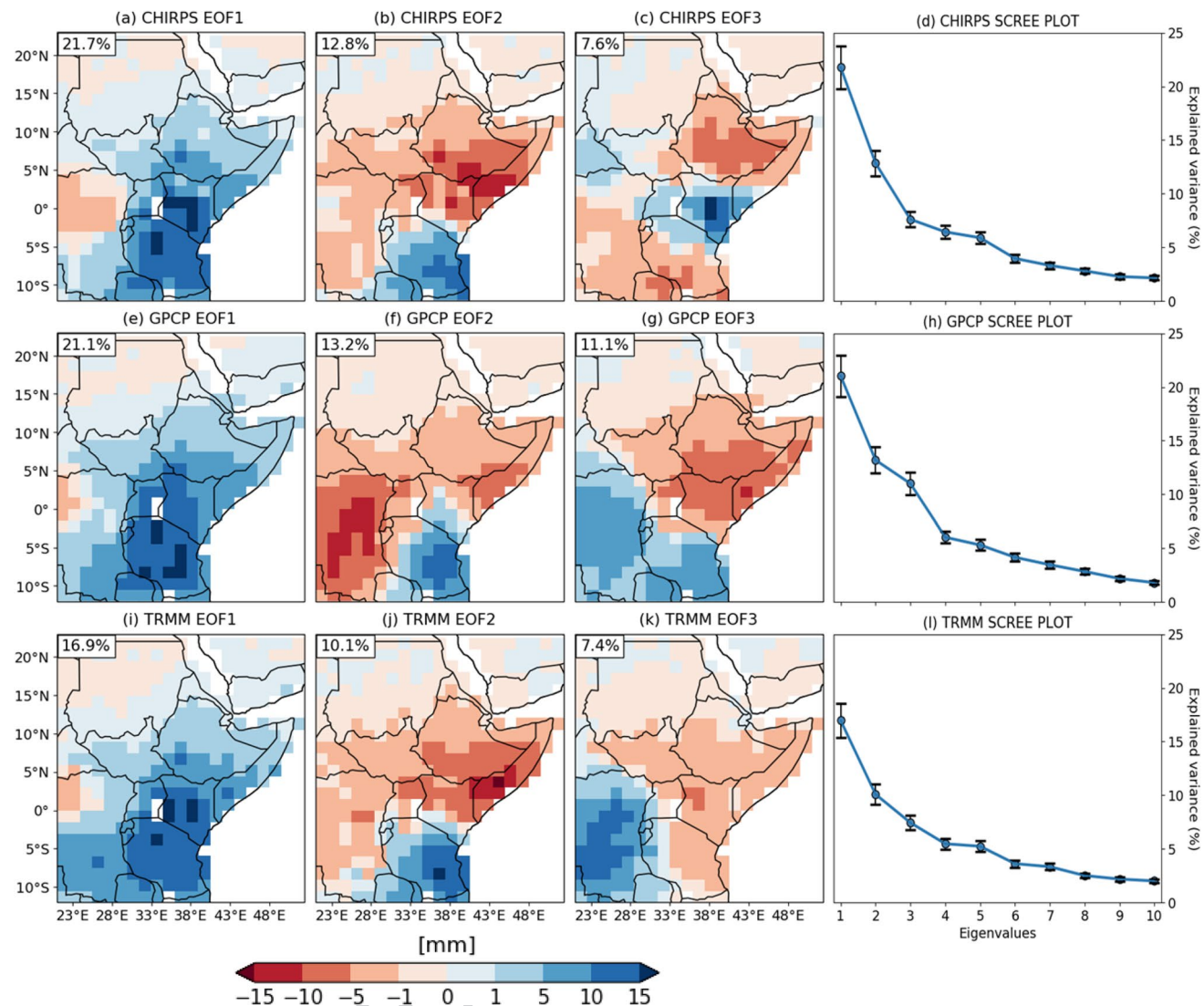


**Fig. 5** The first three spatial EOF modes (or eigenvectors) for weekly (a)-(c) CHIRPS, (e)-(g) GPCP, and (i)-(k) TRMM rainfall accumulation anomalies during OND, with their explained variance in percentage (%) shown in the top-left corner. Scree plot showing the corresponding explained variance in percentage (%) for the first ten

eigenvalues of the EOF analysis from weekly (d) CHIRPS, (h) GPCP, and (l) TRMM rainfall anomalies. Sample errors are indicated by the error bars in (d, h, l) according to the North's rule of thumb. Rainfall accumulations are in millimetres (mm)

568 of one to four weeks ahead, respectively. Even though the  
 569 amplitude of anomalies reduces with increasing lead time,  
 570 all models can satisfactorily represent essential characteristics  
 571 of the leading RSMs, that is, the monopole-like rainfall  
 572 pattern for RSM1 (Fig. 7) and the dipole-like rainfall pattern  
 573 for RSM2 (Fig. 8), in agreement with the observations (con-  
 574 tours in Figs. 7, 8). The ability of the NCEP model to capture  
 575 RSM1 and RSM2 is lower than in other models, as indicated  
 576 by the largest region-averaged amplitude differences and the  
 577 weakest spatial correlation coefficients computed between  
 578 modelled and observed RSMs. Less accurate outcomes in  
 579 the NCEP model are, in particular, associated with errors in  
 580 representing the location of the rainfall anomaly. For RSM1,

581 this is seen through the largest positive anomalies displaced  
 582 to the west of Tanzania (Figs. 7e, f, g, h) compared to the  
 583 ECMWF (Figs. 7a, b, c, d) and UKMO (Figs. 7i, j, k, l) mod-  
 584 els. ECMWF and UKMO models place such variations in  
 585 rainfall over the entire southeastern sector of Eastern Africa,  
 586 as also seen in the observations. For RSM2, the discrepancy  
 587 is found in the largest negative anomalies (Figs. 8e, f, g, h),  
 588 which appear further to the west of the domain compared to  
 589 the other models and observations (Figs. 8a, b, c, d, i, j, k, l).

590 Shortcomings in capturing the leading RSMs are likely  
 591 related to the model capability of representing its climatol-  
 592 ogy and variance (Online Resource 1—Figs. 2, 3). Although  
 593 all models predict the highest climatological rainfall totals in

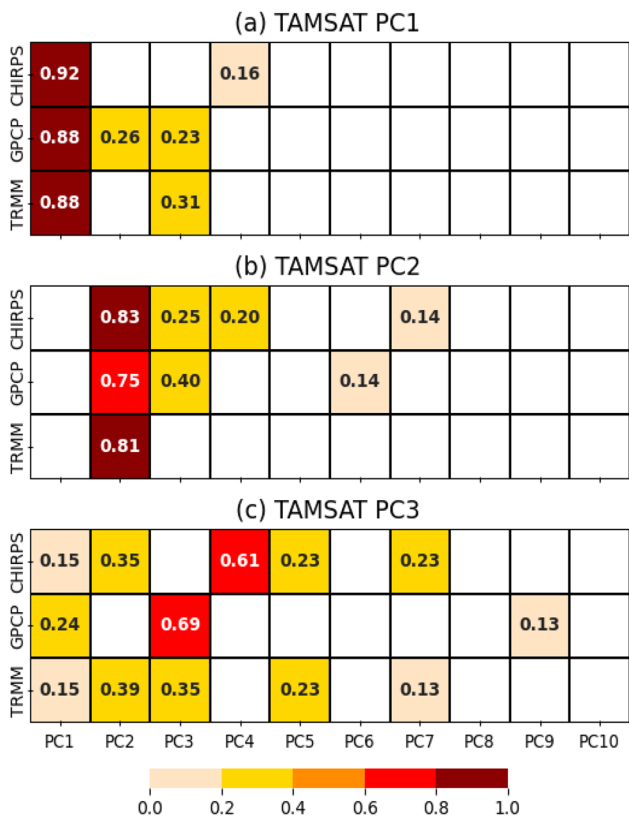


**Fig. 6** Absolute Pearson's correlation for TAMSAT (a) PC1, (b) PC2, and (c) PC3 against the first ten PCs (PC1 to PC10) from CHIRPS, GPCP, and TRMM datasets. Shaded boxes with numbers indicate statistically significant values at the 95% confidence level according to a two-tailed Student's t-test

the western portion of the domain, the mean state response for ECMWF and UKMO (NCEP) is stronger (weaker) than TAMSAT over most of the southern and southeastern sectors of Eastern Africa (compare Fig. 2a with Online Resource 1—Fig. 2). Additionally, all models show a reduction in rainfall variability with increasing lead time, as well as discrepancies at predicting the location of rainfall anomalies, particularly in the NCEP model, which shows higher deviations near DRC compared to TAMSAT (compare Fig. 2b with Online Resource 1—Fig. 3).

The model skill at predicting the leading PCs (PC1 and PC2) in Weeks 1–4 is evaluated in Fig. 9. For both PCs, the skill reduces with increasing lead time, with, in particular, Week 1 showing the highest associations (Fig. 9a) and lowest amplitude errors (Fig. 9b) for all models PC1. UKMO and ECMWF PC1 have the highest skill at all leads, with UKMO having a marginally higher skill than ECMWF. The results for PC1 overall corroborate the correlation assessments performed by de Andrade et al. (2021) for weekly Eastern Africa rainfall anomalies initialised in September–October–November. All models exhibit higher skill at predicting PC1 compared with PC2. Notably, the skill for

NCEP PC1 remains just slightly higher than for ECMWF or UKMO PC2 in Weeks 3–4, and even comparable to these models PC2 in Week 2. The lowest skill is seen for NCEP PC2 at most leads, showing, for instance, a non-significant correlation with a value below 0.2 at Week 4 (Fig. 9a).

## 4 Sources of predictability

To investigate where the skill found in the previous section comes from, Figs. 10 and 11 show respectively the percentage change in the correlations for ECMWF PC1 and PC2 against the corresponding observed PCs considering two conditions: i) when the co-variability between modelled rainfall anomalies and specific climate drivers' indices is subtracted from the model (Figs. 10a, 11a) and (ii) when the corresponding observed co-variability is added to the model (Figs. 10b, 11b) after removing its modelled co-variability as in (i). According to Eq. (1), both conditions (i) and (ii) are relative to reference values obtained when no modification is considered in the model rainfall anomalies before computing the PCs. Since ECMWF and UKMO had comparative skill in Fig. 9, with skill significantly higher than NCEP, the former is used here to compare the results with those found in de Andrade et al. (2021).

The driver-rainfall co-variability subtracted from modelled rainfall anomalies modulates the skill at predicting PC1 (Fig. 10a) and PC2 (Fig. 11a) throughout the lead times. When examining the removal of a single driver's signal rather than a combination of two or more of these drivers' signals in the model, the skill degradation (i.e., negative percentage change) for PC1 is mainly seen after removing the RMM2 signal from hindcasts (Fig. 10a). This shows a correlation reduction varying from 9.3% in Week 1 to 53.8% in Week 4 relative to reference values (i.e., CORR in Fig. 10a). Removing N3.4\* and DMI\* signals from hindcasts also affects the PC1 skill. Nevertheless, the rate of skill degradation over the weeks is no higher than 11.6% for N3.4\* and 15.2% for DMI\* about reference values (Fig. 10a). For PC2 (Fig. 11a), the highest skill degradations occur when removing RMM1- and DMI\*-related rainfall anomalies from hindcasts, with skill reducing over the weeks up to 31.5% and 36.2%, respectively, comparing to reference values (i.e., CORR in Fig. 11a). When all drivers' signals are eliminated from the model, the overall skill drop estimated is substantially explained by skill degradation associated with the removal of the MJO signal from hindcasts (compare RMM2 and RMM1 with ALL in Figs. 10a and 11a, respectively), which is more pronounced for PC1 than for PC2 (compare RMM2 in Fig. 10a with RMM1 in Fig. 11a). These decreases in skill seen when subtracting all drivers' signals from hindcasts are also considerably associated with removing the DMI\* signal in the model, particularly for PC2

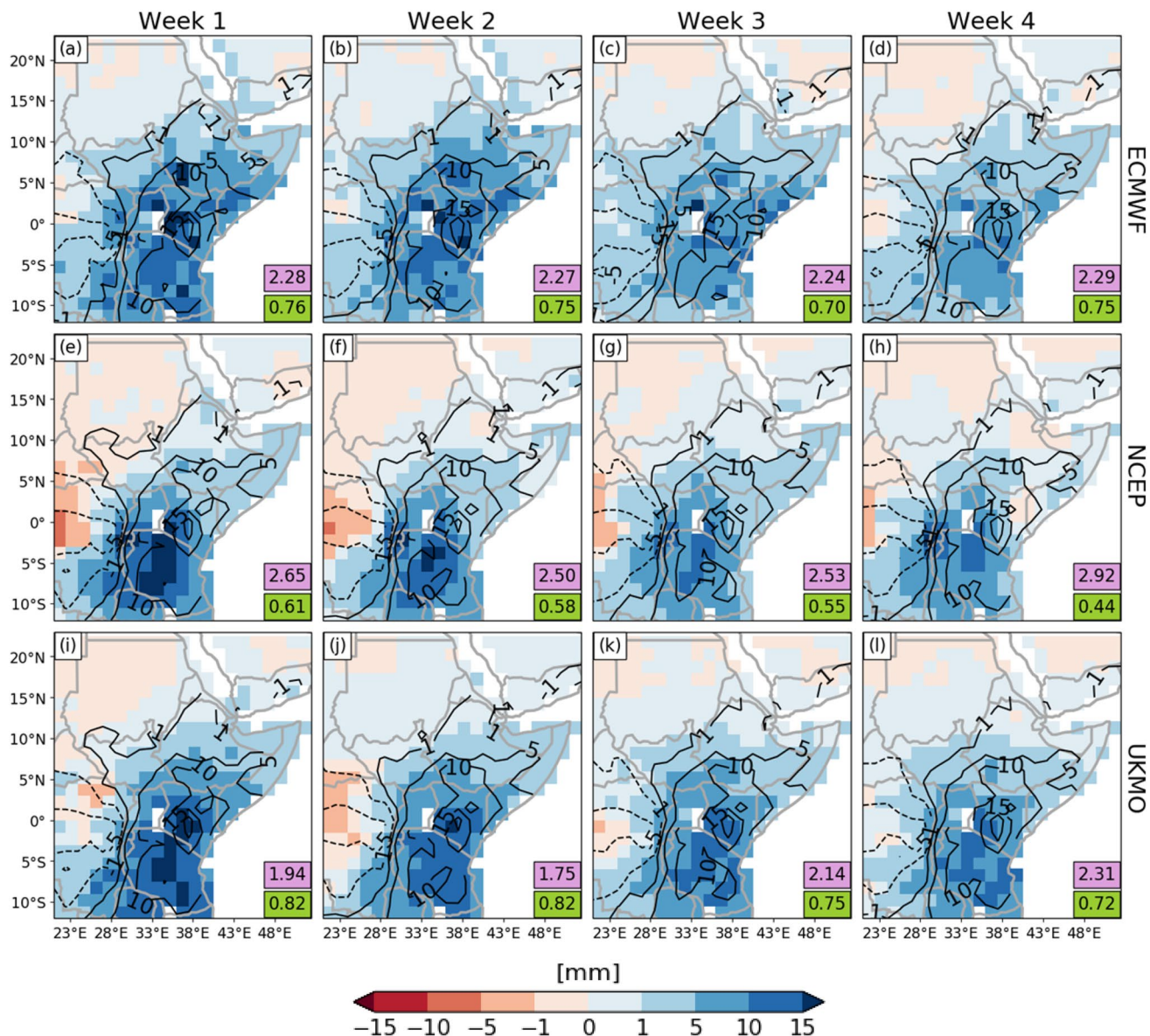


**Fig. 7** First regressed spatial mode (RSM1) at Weeks 1–4 for (a)–(d) ECMWF, (e)–(h) NCEP, and (i)–(l) UKMO models (shaded). The contours denote the corresponding RSM for TAMSAT rainfall anomalies, with solid (dashed) lines for positive (negative) values. The zero line is omitted. Magenta (Green) boxes in the bottom-right corner

indicate the region-averaged absolute difference (statistically significant spatial correlation) between modelled and observed RSMs. Statistically significant spatial correlation at the 95% level confidence level is examined according to a two-tailed Student's t-test

666 (compare DMI\* with ALL in Figs. 10a, 11a). The combined  
 667 removal of rainfall variations linked to RMM components  
 668 (RMM1+RMM2) and SST indices (N3.4\*+DMI\*) further  
 669 indicates that degradations in PC1 forecast skill are mainly  
 670 related to the RMM2 signal, and are secondarily associated  
 671 with N3.4\* and DMI\* signals (Fig. 10a). For PC2,  
 672 however, such a combined removal affecting its prediction  
 673 skill is dominated by RMM1 and DMI signals in the model  
 674 (Fig. 11a). Thus, these forecast skill results for PC1 and PC2  
 675 corroborate the corresponding observed associations shown  
 676 in Fig. 3.

677 Skill improvements (i.e., positive percentage changes)  
 678 are seen for both PC1 and PC2 predictions after replacing  
 679 the modelled rainfall response to a single driver with the  
 680 corresponding observed response, especially in Weeks 3–4 (Figs. 10b, 11b). Although PC1 and PC2  
 681 skills improve if using corrected DMI\*-related rainfall  
 682 variability patterns, this approach is not more effective  
 683 than simply correcting the model with the observed  
 684 MJO-related rainfall variability. Moreover, the effect of  
 685 adjusting the rainfall signal associated with N3.4\* in the  
 686 model is almost zero (Figs. 10b, 11b), indicating that of  
 687

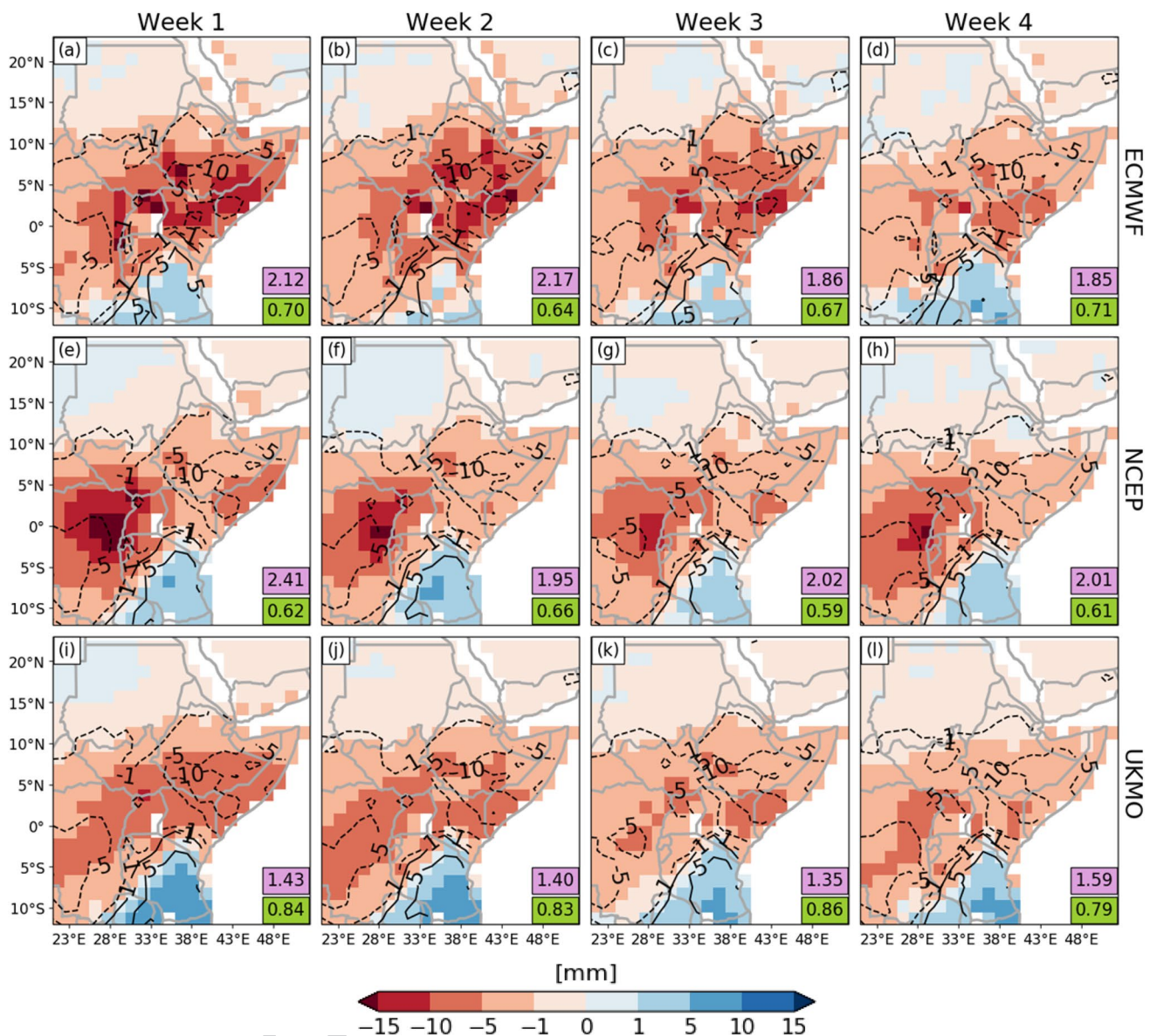


**Fig. 8** Second regressed spatial mode (RSM2) at Weeks 1–4 for (a)–(d) ECMWF, (e)–(h) NCEP, and (i)–(l) UKMO models (shaded). The contours denote the corresponding RSM for TAMSAT rainfall anomalies, with solid (dashed) lines for positive (negative) values. The zero line is omitted. Magenta (Green) boxes in the bottom-right corner

indicate the region-averaged absolute difference (statistically significant spatial correlation) between modelled and observed RSMs. Statistically significant spatial correlation at the 95% level confidence level is examined according to a two-tailed Student's t-test

the predictability drivers investigated here, ENSO contributes the least to varying PCs forecast skill. PC1 skill improvements are more sensitive to RMM2 variations than to anomalies in other drivers (Fig. 10b), whereas the most pronounced PC2 skill responses are linked to RMM1 variations (Fig. 11b). These findings are supported, for example, by the largest positive percentage changes for PC1 and PC2 in Week 4, with correlation coefficients exceeding, respectively, 50% (RMM2 in Fig. 10b) and 70% (RMM1 in Fig. 11b) relative to reference values (i.e., CORR in Figs. 10b, 11b). For PC2 rather than PC1, skill

improvements associated with MJO are more pronounced (compare RMM1 in Fig. 11b with RMM2 in Fig. 10b), and account for a considerable portion of the enhanced overall level of skill after including all observed drivers' signals in the model (compare RMM1 and RMM2 with ALL in Figs. 11b and 10b, respectively).

The results presented in this section overall corroborate the ones found by de Andrade et al. (2021), highlighting, in particular, the potential contribution of improved

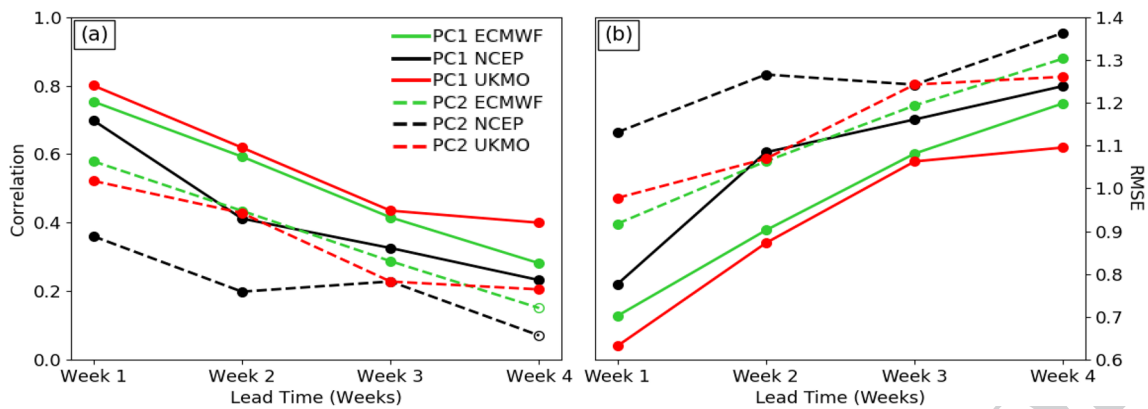


**Fig. 9** (a) Correlation and (b) RMSE for the first two observed (TAMSAT) and modelled (ECMWF, NCEP, and UKMO) PCs (PC1 and PC2) at Weeks 1–4. Solid (Dashed) lines indicate the skill assess-

ment for PC1 (PC2). The open circle marker in (a) denotes correlation coefficients that are not statistically significant at the 95% level confidence level according to a two-tailed Student's t-test

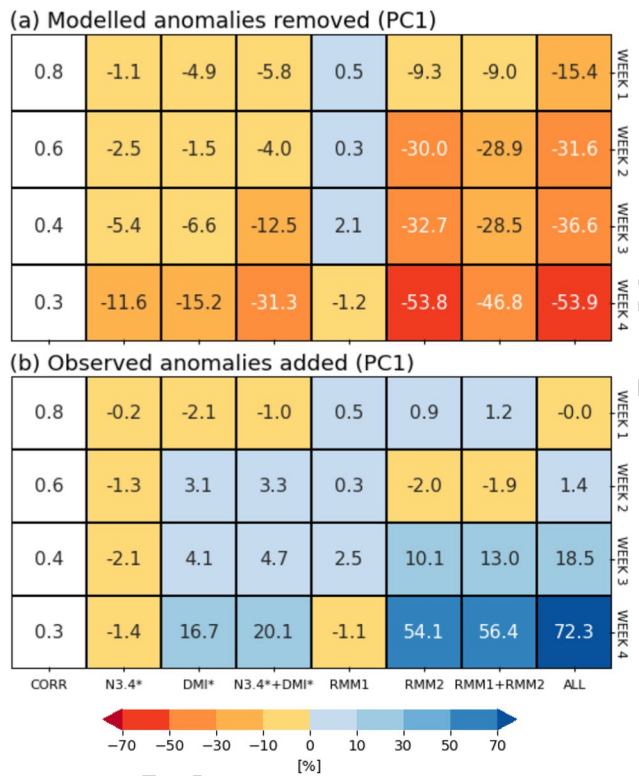


**Fig. 10** Percentage change in the correlation between TAMSAT and ECMWF PC1 at Weeks 1–4 computed after (a) removing from and (b) adding to model rainfall anomalies a particular driver-related variability. The co-variability is indicated at the bottom of (b) by the corresponding driver's index or a combination of two or all ("ALL") drivers' indices. The leftmost column shows the correlation computed without modifying any driver-related signal in rainfall anomalies ("CORR"), as in Fig. 9a (solid green line)

MJO-related rainfall variability (or a bias correction based

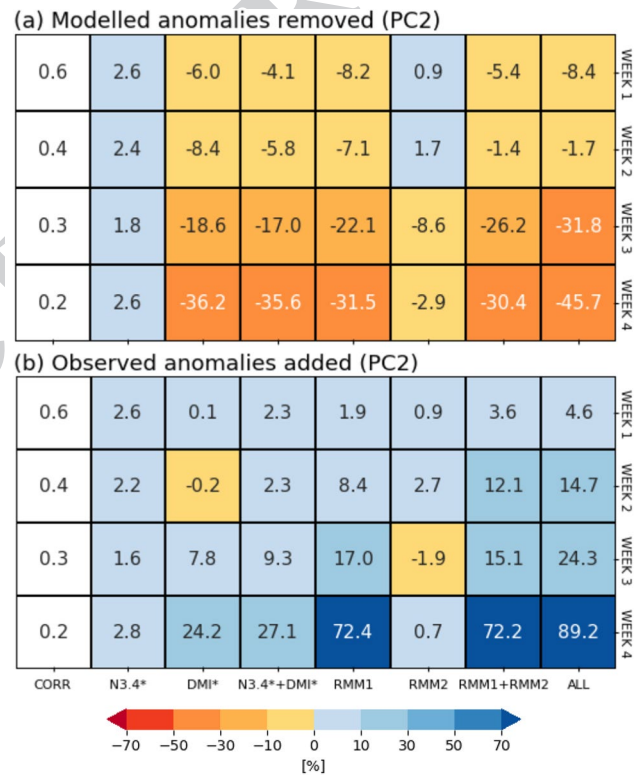


**Fig. 11** Percentage change in the correlation between TAMSAT and ECMWF PC2 at Weeks 1–4 computed after (a) removing from and (b) adding to model rainfall anomalies a particular driver-related variability. The co-variability is indicated at the bottom of (b) by the corresponding driver's index or a combination of two or all ("ALL") drivers' indices. The leftmost column shows the correlation computed without modifying any driver-related signal in rainfall anomalies ("CORR"), as in Fig. 9a (dashed green line)

on the MJO impacts on model rainfall anomalies) to skill increases in weekly Eastern Africa rainfall predictions within the ECMWF model.

## 711 5 Summary and conclusions

712 The sub-seasonal variability and prediction skill of short  
 713 rains in Eastern Africa are assessed using several observational  
 714 and model datasets. An EOF analysis is performed  
 715 to identify the leading modes of weekly rainfall variability  
 716 in Eastern Africa, allowing exploring their associations  
 717 with specific climate drivers. This study then goes on to  
 718 investigate the ability of dynamical models to capture and  
 719 predict the leading rainfall modes, as well as examine  
 720 potential-related sources of predictability.

721 Irrespective of the observational dataset used (i.e.,  
 722 TAMSAT, CHIRPS, GPCP, or TRMM), two distinct  
 723 weekly rainfall modes in the Eastern African short rains  
 724 from October to December (OND) are identified; these are:  
 725 i) a monopole-like rainfall pattern with the largest anomalies  
 726 in southern Ethiopia, Kenya, and northern Tanzania; and (ii) a dipole-like rainfall pattern between Tanzania and  
 727 the northeastern sector of Eastern Africa, mainly impacting  
 728 Ethiopia and Somalia. Our results indicated that the  
 729 two leading rainfall modes have the strongest correlations  
 730 with the MJO. Specifically, the first (second) rainfall mode  
 731 showed the highest correlations with the RMM2 (RMM1)  
 732 index, which is linked to MJO-related convective anomalies  
 733 in the tropical Indian Ocean and western Pacific (Mar-  
 734itime Continent and Western Hemisphere). Moreover, we  
 735 found that the first and second leading modes are signifi-  
 736 cantly correlated with the DMI index, with the former also  
 737 having significant associations with the N3.4 index if the  
 738 ENSO-IOD co-variability is retained in the index. Despite  
 739 using distinct datasets, periods, domains, and methods for  
 740 representing ENSO and IOD activities, our results com-  
 741plement previous work (e.g., Bowden and Semazzi 2007),  
 742 suggesting that the modulation of the leading weekly rain-  
 743 fall modes may depend on the MJO variability superim-  
 744 posed on distinct lower-frequency background conditions,  
 745 which deserves additional investigation.

746 The ability of ECMWF, NCEP, and UKMO models to  
 747 capture and predict the two leading rainfall modes at lead  
 748 times of one to four weeks is also examined. Evaluation  
 749 of modelled spatiotemporal properties of rainfall modes  
 750 showed that ECMWF and UKMO are comparable and  
 751 outperformed NCEP. NCEP exhibited, with respect to  
 752 observations, a westward shift in the anomalies of both  
 753 spatial modes, which may explain the model shortcomings  
 754 in capturing the rainfall associated with those modes. The  
 755 skill assessments for predicting the corresponding PCs  
 756 further demonstrated that models' phase and amplitude  
 757 errors increased from Week 1 to Week 4, with ECMWF  
 758 and UKMO PC1 having the highest skill at all lead times  
 759 and PC2 showing lower skill than PC1 for all models.

761 To improve the understanding of potential sources driv-  
 762 ing ECMWF model skill, an examination of specific cli-  
 763 mate drivers in modulating the model ability to predict the  
 764 leading rainfall modes is further carried out. We showed  
 765 evidence that if the modelled MJO-related rainfall variability  
 766 is removed from the model, this leads to a degradation in  
 767 predicting the leading PCs, with rainfall variations linked  
 768 to the RMM2 (RMM1) index contributing the most to the  
 769 percentage change in the PC1- (PC2-) related skill. We also  
 770 found that removing SST-related rainfall variations in the  
 771 model modulates skill reductions in both PCs, with ENSO  
 772 and IOD (IOD) impacting the skill at predicting PC1 (PC2).  
 773 Skill degradations are mainly compensated after replacing  
 774 the modelled MJO-related rainfall variability with observed  
 775 MJO-related rainfall variability in the model, leading to the  
 776 largest skill improvements in Weeks 3–4. It is worth noting  
 777 that the skill for PC1 and PC2 is respectively improved by  
 778 up to 18.2% and 16.8% over the weeks when considering the  
 779 combination of all corrected driver-related rainfall variabil-  
 780 ity relative to considering the most correlated MJO signal  
 781 only (i.e., RMM2 for PC1 and RMM1 for PC2). Thus, our  
 782 results indicate that correcting SST-related rainfall vari-  
 783 ations in the model, especially those associated with IOD,  
 784 could have contributed to enhancing the skill in predicting  
 785 the leading rainfall modes, though suggesting a secondary  
 786 role.

787 Even though it is still challenging to predict sub-seasonal  
 788 variations in Eastern Africa short rains (de Andrade et al.  
 789 2021; Kolstad et al. 2021), this study demonstrated, in par-  
 790 ticular, that strengthening the model ability to capture MJO-  
 791 related rainfall variability has the potential to more accu-  
 792 rately predict the main modes of weekly rainfall variability  
 793 in the region. These results support the concept of windows  
 794 of opportunity (Mariotti et al. 2020) that may help forecast-  
 795 ers identify periods when sub-seasonal rainfall prediction  
 796 accuracy is at its highest during Eastern Africa short rains.  
 797 Additionally, given that the drivers examined interact with  
 798 each other (e.g., Hendon et al. 2007; Wilson et al. 2013;  
 799 Zhang et al. 2015) and that their combined activity may  
 800 impact the rainfall in Eastern Africa during the short rains  
 801 (e.g., Vashisht and Zaitchik 2022), future work is recom-  
 802 mended to specifically elucidate the multi-way interactions  
 803 among ENSO, IOD, and the MJO, as well as the correspond-  
 804 ing effects on the sub-seasonal Eastern Africa short rains  
 805 prediction skill. However, when examining forecast skill,  
 806 the limited length of typical hindcast datasets can limit the  
 807 number of samples of each combination of phases of mul-  
 808 tiple drivers.

809 Finally, by projecting sub-seasonal rainfall anomaly fore-  
 810 casts onto the two observed leading rainfall modes examined  
 811 here, a pair of sub-seasonal rainfall monitoring indices could  
 812 be used as a forecasting tool in operational routines across  
 813 Eastern Africa. Therefore, in addition to supporting model

814 developers in identifying shortcomings in Eastern Africa  
 815 rainfall predictions for advancing the sub-seasonal prediction  
 816 systems in the future, our results can further contribute  
 817 to developing sub-seasonal forecast products that may  
 818 add valuable climate information for anticipatory planning  
 819 decisions across several sectors, such as agriculture, food  
**AQ5** security, and energy.

821 **Acknowledgements** We thank TAMSAT, The Climate Hazards  
 822 Center, the National Center for Atmospheric Research, the National  
 823 Aeronautics and Space Administration, the International Research  
 824 Institute for Climate and Society, ECMWF, and NOAA for data provi-  
 825 sion. This work is based on S2S data. S2S is a joint initiative of the  
 826 World Weather Research Programme (WWRP) and the World Climate  
 827 Research Programme (WCRP). The original S2S database is hosted at  
 828 ECMWF as an extension of the TIGGE database.

829 **Author contributions** All authors contributed to the study conception,  
 830 design, and analysis. Material preparation and data collection were per-  
 831 formed by Felipe Marques de Andrade. The first draft of the manuscript  
 832 was written by Felipe Marques de Andrade and all authors commented  
 833 on previous versions of the manuscript. All authors read and approved  
 834 the final manuscript.

835 **Funding** FMdeA, LCH, and SJW were supported by the U.K. Research  
 836 and Innovation as part of the GCRF, African SWIFT Programme (NE/  
 837 P021077/1). LCH and SJW were also supported by the National Centre  
 838 for Atmospheric Science through the NERC National Capability  
 839 International Programmes Award (NE/X006263/1).

840 **Data availability** The data used in this research can be found at the fol-  
 841 lowing websites: TAMSAT (<http://www.tamsat.org.uk/data/>); CHIRPS  
 842 ([https://data.cse.ucsb.edu/products/CHIRPS-2.0/global\\_daily/netcdf/p05/](https://data.cse.ucsb.edu/products/CHIRPS-2.0/global_daily/netcdf/p05/)); GPCP (<https://rda.ucar.edu/datasets/ds728.7/>); TRMM ([https://disc2.gesdisc.eosdis.nasa.gov/opendap/TRMM\\_L3/TRMM\\_3B42\\_Daily.7/](https://disc2.gesdisc.eosdis.nasa.gov/opendap/TRMM_L3/TRMM_3B42_Daily.7/)); S2S hindcasts (<https://apps.ecmwf.int/datasets/>); RMM index (<https://aux.ecmwf.int/ecpds/data/list/RMMS/> (username: s2sidx; password: s2sidx)); SubX hindcasts ([https://iridl.ldeo.columbia.edu/SOURCES/Models/\\_SubX/NCEP/CFSv2/hindcast/pr/](https://iridl.ldeo.columbia.edu/SOURCES/Models/_SubX/NCEP/CFSv2/hindcast/pr/)); SST (<https://psl.noaa.gov/data/gridded/data.noaa.oisst.v2.highres.html>).

850 **Code availability (software application or custom code)** The python  
 851 codes used in this research are available upon request to the first author.

## 852 **Declarations**

853 **Competing interests** The authors declare no conflicts of interest.

## AQ6 AQ7 **References**

855 Aageet S, Fink AH, Maranan M, Diem JE, Hartter J, Ssali AL, Aya-  
 856 bagabo P (2022) Validation of satellite rainfall estimates over  
 857 equatorial east Africa. *J Hydrometeorol* 23:129–151. <https://doi.org/10.1175/JHM-D-21-0145.1>

858 Allen MP (1997) The t-test for the simple regression coefficient. *Under-  
 859 standing Regression Analysis*, Springer, 66–70. [https://doi.org/10.1007/978-0-585-25657-3\\_14](https://doi.org/10.1007/978-0-585-25657-3_14)

860 Anande D, Luhunga P (2019) Assessment of Socio-Economic Impacts  
 861 of the December 2011 Flood Event in Dar es Salaam, Tanzania.  
 862 *Atmospheric Climate Sci* 9:421–437. <https://doi.org/10.4236/acs.2019.93029>

863 Bahaga TK, Mengistu Tsidu G, Kucharski F, Diro GT (2015) Poten-  
 864 tial predictability of the sea-surface temperature forced equato-  
 865 rial East African short rains interannual variability in the 20th  
 866 century. *Quart J Roy Meteorol Soc* 141:16–26. <https://doi.org/10.1002/qj.2338>

867 Bahaga TK, Fink AH, Knippertz P (2019) Revisiting interannual  
 868 to decadal teleconnections influencing seasonal rainfall in the  
 869 Greater Horn of Africa during the 20th century. *Int J Climatol*  
 870 39:2765–2785. <https://doi.org/10.1002/joc.5989>

871 Behera SK, Luo JJ, Masson S, Delecluse P, Gualdi S, Navarra A,  
 872 Yamagata T (2005) Paramount impact of the Indian Ocean  
 873 dipole on the East African short rains: A CGCM study. *J Clim*  
 874 18:4514–4530. <https://doi.org/10.1175/JCLI3541.1>

875 Bergonzini L, Richard Y, Petit L, Camberlin P (2004) Zonal circula-  
 876 tions over the Indian and Pacific oceans and the level of lakes  
 877 Victoria and Tanganyika. *Int J Climatol* 24:1613–1624. <https://doi.org/10.1002/joc.1089>

878 Berhane F, Zaitchik B (2014) Modulation of daily precipitation over  
 879 East Africa by the Madden–Julian oscillation. *J Clim* 27:6016–  
 880 6034. <https://doi.org/10.1175/JCLI-D-13-00693.1>

881 Black E, Slingo J, Sperber KR (2003) An observational study of the  
 882 relationship between excessively strong short rains in coastal  
 883 East Africa and Indian Ocean SST. *Mon Weather Rev* 131:74–  
 884 94. [https://doi.org/10.1175/1520-0493\(2003\)131%3c0074:AOSOTR%3e2.0.CO;2](https://doi.org/10.1175/1520-0493(2003)131%3c0074:AOSOTR%3e2.0.CO;2)

885 Bowden JH, Semazzi FH (2007) Empirical analysis of intraseasonal  
 886 climate variability over the Greater Horn of Africa. *J Clim*  
 887 20:5715–5731. <https://doi.org/10.1175/2007JCLI1587.1>

888 Camberlin P, Wairuto J (1997) Intraseasonal wind anomalies related  
 889 to wet and dry spells during the “long” and “short” rainy sea-  
 890 sons in Kenya. *Theor Appl Climatol* 58:57–69. <https://doi.org/10.1007/BF00867432>

891 Camberlin P, Moron V, Okoola RE, Philippon N, Gitau W (2009)  
 892 Components of rainy seasons’ variability in equatorial East  
 893 Africa: Onset, cessation, rainfall frequency and intensity.  
 894 *Theor Appl Climatol* 98:237–249. <https://doi.org/10.1007/s00704-009-0113-1>

895 Chang'a L, Kijazi A, Mafuru K, Kondowe A, Osima S, Mtongori H,  
 896 Ng'ongolo H, Juma O, Michael E (2020) Assessment of the Evo-  
 897 lution and Socio-Economic Impacts of Extreme Rainfall Events  
 898 in October 2019 over the East Africa. *Atmospheric Climate Sci*  
 899 10:319–338. <https://doi.org/10.4236/acs.2020.103018>

900 de Andrade FM, Young MP, MacLeod D, Hiron LC, Woolnough SJ,  
 901 Black E (2021) Subseasonal precipitation prediction for Africa:  
 902 Forecast evaluation and sources of predictability. *Weather Fore-  
 903 cast* 36:265–284. <https://doi.org/10.1175/WAF-D-20-0054.1>

904 Dinku T, Ceccato P, Grover-Kopec E, Lemma M, Connor SJ,  
 905 Ropelewski CF (2007) Validation of satellite rainfall products over  
 906 East Africa’s complex topography. *Int J Remote Sens* 28:1503–  
 907 1526. <https://doi.org/10.1080/01431160600954688>

908 Dinku T, Ceccato P, Connor SJ (2011) Challenges of satellite rainfall  
 909 estimation over mountainous and arid parts of east Africa. *Int J  
 910 Remote Sens* 32:5965–5979. <https://doi.org/10.1080/01431161.2010.499381>

911 FSNAU (Somalia) Food Security & Nutrition Quarterly Brief (2022)  
 912 — Focus on Post Gu 2017 Season Early Warning (Food Security  
 913 and Nutrition Analysis Unit and Famine Early Warning System  
 914 Network)

915 Funk C, Dettinger MD, Michaelsen JC, Verdin JP, Brown ME, Barlow  
 916 M, Hoell A (2008) Warming of the Indian Ocean threatens east-  
 917 ern and southern African food security but could be mitigated by  
 918 agricultural development. *Proc Natl Acad Sci* 105:11081–11086.  
 919 <https://doi.org/10.1073/pnas.070819610>

920 Funk C, Peterson P, Landsfeld M, Pedreros D, Verdin J, Shukla S,  
 921 Husak G, Rowland J, Harrison L, Hoell A, Michaelsen J (2015)  
 922 The climate hazards infrared precipitation with stations—a new  
 923

924

925

926

927

928

929

930

931

932 environmental record for monitoring extremes. *Sci Data* 2:150066. 998  
 933 <https://doi.org/10.1038/sdata.2015.66> 999

934 Gamoyo M, Reason C, Obura S (2015) Rainfall variability over the 1000  
 935 East African coast. *Theor Appl Climatol* 120:311–322. <https://doi.org/10.1007/s00704-014-1171-6> 1001

936 Goddard L, Graham NE (1999) Importance of the Indian Ocean for 1002  
 937 simulating rainfall anomalies over eastern and southern Africa. *J 1003  
 938 Geophys Res Atmos* 104:19099–19116. [https://doi.org/10.1029/1999JD900326](https://doi.org/10.1029/1004<br/>
  939 1999JD900326) 1004

940 Gudoshava M, Wanzala M, Thompson E, Mwesigwa J, Endris HS, 1005  
 941 Segele Z, Hiron L, Kipkoge O, Mumbua C, Njoka W, Baraibar 1006  
 942 M, de Andrade FM, Woolnough SJ, Atheru Z, Artan G (2022) 1007  
 943 Application of real-time S2S forecasts over Eastern Africa in the 1008  
 944 co-production of climate services. *Climate Services* 27:100319. 1009  
 945 <https://doi.org/10.1016/j.cleser.2022.100319> 1010

946 Hannachi A, Jolliffe IT, Stephenson DB (2007) Empirical orthogonal 1011  
 947 functions and related techniques in atmospheric science: A review. 1012  
 948 *Int J Climatol: J Royal Meteorol Soc* 27:1119–1152. <https://doi.org/10.1002/joc.1499> 1013

949 Hendon HH, Wheeler MC, Zhang C (2007) Seasonal dependence of 1014  
 950 the MJO–ENSO relationship. *J Clim* 20:531–543. <https://doi.org/10.1175/JCLI4003.1> 1015

951 Hersbach H et al (2020) The ERA5 global reanalysis. *Q J R Meteorol 1016  
 952 Soc* 146:1999–2049. <https://doi.org/10.1002/qj.3803> 1017

953 Hiron L, Turner A (2018) The impact of Indian Ocean mean-state 1018  
 954 biases in climate models on the representation of the East African 1019  
 955 short rains. *J Clim* 31:6611–6631. <https://doi.org/10.1175/JCLI-D-17-0804.1> 1020

956 Hiron L, Thompson E, Dione C, Indasi VS, Kilavi M, Nkiaka E, 1021  
 957 Talib J, Visman E, Adefisan EA, de Andrade FM, Ashong J, 1022  
 958 Mwesigwa JB, Boult V, Diédhieu T, Konte O, Gudoshava M, 1023  
 959 Kiptum C, Amoah RK, Lampert B, Lawal KA, Muita R, Nzekwu 1024  
 960 R, Nying'uro P, Ochieng W, Olaniany E, Opoku NK, Endris HS, 1025  
 961 Segele Z, Igri PM, Mwangi E, Woolnough S (2021) Using 1026  
 962 co-production to improve the appropriate use of sub-seasonal 1027  
 963 forecasts in Africa. *Climate Services* 23:100246. <https://doi.org/10.1016/j.cleser.2021.100246> 1028

964 Hoell A, Funk C, Barlow M (2014) La Niña diversity and northwest 1029  
 965 Indian Ocean rim teleconnections. *Clim Dyn* 43:1–18. <https://doi.org/10.1007/s00382-014-2083-y> 1030

966 Hogan E, Shelly A, Xavier P (2015) The observed and modelled 1031  
 967 influence of the Madden–Julian Oscillation on East African rainfall. 1032  
 968 *Meteorol Appl* 22:459–469. <https://doi.org/10.1002/met.1475> 1033

969 Huffman GJ, Adler RF, Morrissey MM, Bolvin DT, Curtis S, Joyce 1034  
 970 R, McGavock B, Susskind J (2001) Global precipitation at one- 1035  
 971 degree daily resolution from multisatellite observations. *J Hydrometeorol* 1036  
 972 2:36–50. 1037

973 Huffman GJ, Bolvin DT, Nelkin EJ, Wolff DB, Adler RF, Gu G, Hong 1038  
 974 Y, Bowman KP, Stocker EF (2007) The TRMM multisatellite 1039  
 975 precipitation analysis (TMPA): Quasi-global, multiyear, combined- 1040  
 976 sensor precipitation estimates at fine scales. *J Hydrometeorol* 1041  
 977 8:38–55. <https://doi.org/10.1175/JHM560.1> 1042

978 Indeje M, Semazzi FHM, Ogallo LJ (2000) ENSO Signals in East 1043  
 979 African Rainfall Seasons. *Int J Climatol* 20:19–46. [https://doi.org/10.1002/\(SICI\)1097-0088\(200001\)20:1%3c19::AID-JOC449%3e3.0.CO;2-0](https://doi.org/10.1002/(SICI)1097-0088(200001)20:1%3c19::AID-JOC449%3e3.0.CO;2-0) 1044

980 Jiang Y, Zhou L, Roundy PE, Hua W, Raghavendra A (2021) Increasing 1045  
 981 influence of Indian Ocean Dipole on precipitation over Central 1046  
 982 Equatorial Africa. *Geophys Res Lett* 48:e2020GL092370. <https://doi.org/10.1029/2020GL092370> 1047

983 Kimani MW, Hoedjes JC, Su Z (2017) An assessment of satellite- 1048  
 984 derived rainfall products relative to ground observations over East 1049  
 985 Africa. *Remote Sensing* 9:430. <https://doi.org/10.3390/rs9050430> 1050

986 Kolstad EW, MacLeod D (2022) Lagged oceanic effects on the East 1051  
 987 African short rains. *Clim Dyn* 59:1043–1056. <https://doi.org/10.1007/s00382-022-06176-6> 1052

988 Ogallo LJ (1989) The spatial and temporal patterns of the East African 1053  
 989 seasonal rainfall derived from principal component analysis. *Int 1054  
 990 J Climatol* 9:145–167. <https://doi.org/10.1002/joc.3370090204> 1055

991 Ogallo LJ, Janowiak JE, Halpert MS (1988) Teleconnection between 1056  
 992 seasonal rainfall over East Africa and global sea surface temperature 1057  
 993 anomalies. *J Meteorol Soc Jpn* 66:807–821. [https://doi.org/10.2151/jmsj1965.66.6\\_807](https://doi.org/10.2151/jmsj1965.66.6_807) 1058

994 Omeny PA, Ogallo L, Okoola R, Hendon H, Wheeler M (2008) East 1059  
 995 African rainfall variability associated with the Madden–Julian 1060  
 996 Oscillation. *J Kenya Meteorol Soc* 2:109–118. 1061

997 Palmer PI, Wainwright CM, Dong B et al (2023) Drivers and impacts 1062  
 998 of Eastern African rainfall variability. *Nat Rev Earth Environ* 4:254–270. <https://doi.org/10.1038/s43017-023-00397-x> 1063

999 Pegion K, Kirtman BP, Becker E, Collins DC, LaJoie E, Burgman 1063

999 R, Bell R, DeSole T, Min D, Zhu Y, Li W et al (2019) The

1064 Subseasonal Experiment (SubX): A multimodel subseasonal pre- 1111  
 1065 diction experiment. *Bull Am Meteor Soc* 100:2043–2060. <https://doi.org/10.1175/BAMS-D-18-0270.1> 1112  
 1066  
 1067 Pohl B, Camberlin P (2006a) Influence of the Madden–Julian Oscil- 1113  
 1068 lation on East African rainfall. I: Intraseasonal variability and 1114  
 1069 regional dependency. *Q. J. R. Meteorol. Soc.*, 132(621), 2521– 1115  
 1070 2539. doi:<https://doi.org/10.1256/qj.05.104>. 1116  
 1071 Pohl B, Camberlin P (2006b) Influence of the Madden–Julian Oscil- 1117  
 1072 lation on East African rainfall: II. March–May season extremes 1118  
 1073 and interannual variability, *Q. J. R. Meteorol. Soc.* 132(621, B), 1119  
 1074 2541–2558. <https://doi.org/10.1256/qj.05.223>. 1120  
 1075 Reynolds RW, Smith TM, Liu C, Chelton DB, Casey KS, Schlax MG 1121  
 1076 (2007) Daily high-resolution-blended analyses for sea surface 1122  
 1077 temperature. *Journal of climate* 15;20(22):5473–96. <https://doi.org/10.1175/2007JCLI1824.1> 1123  
 1078 Saji NH, Goswami BN, Vinayachandran PN, Yamagata T (1999) A 1124  
 1079 dipole mode in the tropical Indian Ocean. *Nature* 401:360–363. 1125  
 1080 <https://doi.org/10.1038/43854> 1126  
 1081 Schreck CJ, Semazzi FHM (2004) Variability of the recent climate 1127  
 1082 of eastern Africa. *Int J Climatol* 24:681–701. <https://doi.org/10.1002/joc.1019> 1128  
 1083 Sylla MB, Giorgi F, Coppola E, Mariotti L (2013) Uncertainties 1129  
 1084 in daily rainfall over Africa: assessment of gridded observation 1130  
 1085 products and evaluation of a regional climate model simulation. *Int J 1131  
 1086 Climatol* 33:1805–1817. <https://doi.org/10.1002/joc.3551> 1132  
 1087 Trenberth KE, Stepaniak DP (2001) Indices of el Niño evolution. *J 1133  
 1088 Clim* 14:1697–1701. [https://doi.org/10.1175/1520-0442\(2001\)014%3c1697:LIOENO%3e2.0.CO;2](https://doi.org/10.1175/1520-0442(2001)014%3c1697:LIOENO%3e2.0.CO;2) 1134  
 1089 Ummenhofer CC, Sen Gupta A, England MH, Reason CJ (2009) 1135  
 1090 Contributions of Indian Ocean sea surface temperatures to enhanced 1136  
 1091 East African rainfall. *J Clim* 22:993–1013. <https://doi.org/10.1175/2008JCLI2493.1> 1137  
 1092 Vashisht A, Zaitchik B (2022) Modulation of East African boreal fall 1138  
 1093 rainfall: combined effects of the Madden–Julian oscillation (MJO) 1139  
 1094 and El Niño–Southern Oscillation (ENSO). *J Clim* 35:2019–2034. 1140  
 1095 <https://doi.org/10.1175/JCLI-D-21-0583.1> 1141  
 1096 Vigaud N, Tippett MK, Robertson AW (2018) Probabilistic skill of 1142  
 1097 subseasonal precipitation forecasts for the East Africa–West Asia 1143  
 1098 sector during September–May. *Wea Forecasting* 33:1513–1532. 1144  
 1099 <https://doi.org/10.1175/WAF-D-18-0074.1> 1145  
 1100 Vigaud N, Tippett MK, Robertson AW (2019) Deterministic skill of 1146  
 1101 subseasonal precipitation forecasts for the East Africa–West Asia 1147  
 1102 sector from September to May. *J. Geophys. Res. Atmos.* 124, 11 1148  
 1103 887–11 896. <https://doi.org/10.1029/2019JD030747> 1149  
 1104 Vitart F (2017) Madden–Julian oscillation prediction and teleconnec- 1150  
 1105 tions in the S2S database. *Quart J Roy Meteor Soc* 143:2210– 1151  
 1106 2220. <https://doi.org/10.1002/qj.3079> 1152  
 1107  
 1108  
 1109  
 1110  
 1111  
 1112  
 1113  
 1114  
 1115  
 1116  
 1117  
 1118  
 1119  
 1120  
 1121  
 1122  
 1123  
 1124  
 1125  
 1126  
 1127  
 1128  
 1129  
 1130  
 1131  
 1132  
 1133  
 1134  
 1135  
 1136  
 1137  
 1138  
 1139  
 1140  
 1141  
 1142  
 1143  
 1144  
 1145  
 1146  
 1147  
 1148  
 1149  
 1150  
 1151  
 1152

**Publisher's Note** Springer Nature remains neutral with regard to jurisdictional claims in published maps and institutional affiliations.

Springer Nature or its licensor (e.g. a society or other partner) holds exclusive rights to this article under a publishing agreement with the author(s) or other rightsholder(s); author self-archiving of the accepted manuscript version of this article is solely governed by the terms of such publishing agreement and applicable law.

Journal:	<b>382</b>
Article:	<b>7244</b>

## Author Query Form

**Please ensure you fill out your response to the queries raised below and return this form along with your corrections**

Dear Author

During the process of typesetting your article, the following queries have arisen. Please check your typeset proof carefully against the queries listed below and mark the necessary changes either directly on the proof/online grid or in the 'Author's response' area provided below

Query	Details Required	Author's Response
<b>AQ1</b>	Please check if affiliations and there respective authors was captured/presented correctly.	
<b>AQ2</b>	Please confirm if the author names are presented accurately and in the correct sequence (given name, middle name/initial, family name). Author 1 Given name: [specify authors given name] Last name [specify authors last name]. Also, kindly confirm the details in the metadata are correct.	
<b>AQ3</b>	References 'FSNAU 2022, s 2019' are cited in text but not provided in the reference list. Please provide references in the list or delete these citations.	
<b>AQ4</b>	Please check if section heads was captured/presented correctly.	
<b>AQ5</b>	Please check backmatter if all the details in the backmatter was captured/presented correctly.	
<b>AQ6</b>	References 'Chang'a et al (2020), FSNAU (Somalia) Food Security Nutrition Quarterly Brief (2022), Pohl and Camberlin (2006b).' are given in list but not cited in text. Please cite in text or delete them from list.	
<b>AQ7</b>	Please provide complete bibliographic details of references: ( FSNAU (Somalia) Food Security & Nutrition Quarterly Brief (2022) Wilks D S (2006) )	